Journal of Sea Research 191 (2023) 102329

Contents lists available at ScienceDirect

Journal of Sea Research

journal homepage: www.elsevier.com/locate/seares

Assessing the coastal protection role of seagrass meadows along a barrier beach, southern Romanian coast

Irina Dinu [a,*], Albert Monclús i Bori [b], Vicente Gràcia [c], Manuel García-León [d,1], Jue Lin-Ye [d,1], Adrian Stănică [a], Agustín Sánchez-Arcilla [c]

[a] National Institute for Marine Geology and Geoecology GeoEcoMar, 23-25 Dimitrie Onciul St., 024053 Bucharest 2, Romania
[b] Department of Civil and Environmental Engineering, Polytechnic University of Catalonia (DECA-UPC), Campus Diagonal Nord, Building C2, 1-3 Jordi Girona St., 08034 Barcelona, Spain
[c] Laboratory of Maritime Engineering, Polytechnic University of Catalonia (LIM-UPC), Campus Diagonal Nord, Building D1, 1-3 Jordi Girona St., 08034 Barcelona, Spain
[d] International Centre for Research of Coastal Resources (CIIRC), 1-3 Jordi Girona St., Mòdul D1, Campus Nord, 08003 Barcelona, Spain

ARTICLE INFO

Keywords:
Seagrass
Barrier beach
Southern Romanian coast
Numerical modelling
Attenuation
Wave energy

ABSTRACT

The presence of seagrass along the Romanian coast is currently seen as an important component of the marine ecosystem. Moreover, seagrass meadows play an additional wave energy dissipation role that has also to be considered among other ecosystem services. Assessing the impact of a seagrass meadow on the local hydrodynamics is needed to present an integrated protection and adaption plan for discussion with local stakeholders and coastal managers. The impact on wave heights of a possible seagrass meadow, located in front of the barrier beach at the Mangalia marsh on the southern Romanian coast, has been analysed using numerical modelling. Several seagrass configurations have been studied, for low and average wave conditions from various directions. The same waves were used after adding a vegetation mask to the analysed domain, to simulate the presence of a seagrass meadow. The results of the numerical simulations were extracted in several output points, located along three transects crossing the vegetation mask. They show the most significant reduction in the calculated wave energy density during a year of 16.6%, occurring within the seagrass meadow. Our results suggest that, for the southern Romanian coast, seagrass could be introduced in coastal protection plans as an additional measure for wave attenuation.

1. Introduction

Nature-based solutions are nowadays considered as a helping measure to reduce wave energy in areas with medium risk of erosion, as they are not designed to resolve hotspots (Ruckelshaus et al., 2016; Sutton-Grier et al., 2018; Ruangpan et al., 2020).

Although there are many studies on seagrass as an important habitat for various species in many parts of the world (Jiang et al., 2020), there is still a need to quantify its effect as coastal protection solution. In this work we address this issue and we attempt to evaluate the impact of a specific seagrass (*Zostera noltei* or *Zostera noltii*) meadow on the wave heights through numerical modelling. This species is normally present on the southern Romanian coastal zone and it is currently regenerating after having undergone a drastic decline as a follow-up of uncontrolled dredging and water transparency reduction, due to anthropogenic activities (Marin et al., 2013; Niţă et al., 2014).

The use of seagrass meadows as a green measure is discussed by many authors, some based on field experiments and others based on wave flume experiments. Table 1 summarizes some of these contributions.

Granata et al., 2001 performed a detailed study on the effect of a *Posidonia oceanica* meadow, located on the northeast coast of Spain, before and after a storm. The results have shown that, even in high-energy conditions, the mean turbulence is reduced and the waves are attenuated by the seagrass canopy.

Nepf et al., 2007 describes the velocity profile in and above a

* Corresponding author.
E-mail addresses: irinadinu@geoecomar.ro (I. Dinu), a.monclus.b@gmail.com (A. Monclús i Bori), vicente.gracia@upc.edu (V. Gràcia), manuel.garcia-leon@upc.edu (M. García-León), jue.lin@upc.edu (J. Lin-Ye), astanica@geoecomar.ro (A. Stănică), agustin.arcilla@upc.edu (A. Sánchez-Arcilla).
[1] Present address: Nologin Consulting SLU, NOW Systems, Avenida de las Ranillas, 1D, 50018 Zaragoza, Spain.

https://doi.org/10.1016/j.seares.2022.102329
Received 16 June 2022; Received in revised form 24 December 2022; Accepted 26 December 2022
Available online 27 December 2022

Table 1
Contributions on seagrass as a green measure.

Author(s)	Main contributions
Field scale	
Granata et al., 2001	effect of a *Posidonia oceanica* meadow before and after storm
Möller and Spencer, 2002; Möller, 2006; Feagin et al., 2011; Jadhav et al., 2013; Foster-Martinez et al., 2018	wave energy dissipation by saltmarsh vegetation
Newell and Koch, 2004	significant wave reduction for high vegetation densities
Chen et al., 2007; Sierra et al., 2017; Donatelli et al., 2019	numerical modelling to simulate wave damping
Bradley and Houser, 2009; Paul and Amos, 2011	wave attenuation depending on the season and hydrodynamics
Koch et al., 2009	wave attenuation across different coastal vegetated habitats
Infantes et al., 2012; Luhar et al., 2013	wave-induced flows within a meadow of *Posidonia oceanica*
Ganthy et al., 2013a	1-year field survey of *Zostera noltei* meadows SW France
Laboratory scale	
Price et al., 1968; Asano et al., 1993	waves over vegetation simulated by polypropylene fibres
Fonseca et al., 1982; Fonseca and Cahalan, 1992; Larkum et al., 2006	wave energy reduction over several types of seagrass
Mendez et al., 1999; Mendez and Losada, 2004; Lowe et al., 2007	modelling for wave transformation on vegetation fields
Ciraolo et al., 2006	flow resistance of *Posidonia oceanica* in shallow water
Myrhaug et al., 2009	estimation of nonlinear wave-induced drag force over a vegetation field
Luhar et al., 2010; Losada et al., 2016	mean wave-induced current within the model seagrass canopy
Sánchez-González et al., 2011; Manca et al., 2012; Koftis et al., 2013	wave height attenuation by submerged *Posidonia oceanica*
Ganthy et al., 2013b; Kombiadou et al., 2014	modelling to calibrate flume experiments with *Zostera noltei*
Ma et al., 2013, 2015; Blackmar et al., 2014	modelling to study wave damping
Möller et al., 2014	wave attenuation by marsh vegetation
Fonseca and Koehl, 2006; Manca et al., 2010; Ros et al., 2014; John et al., 2015; Ganthy et al., 2015; Maza et al., 2016; Luhar et al., 2017; He et al., 2019	impact of various parameters in wave height reduction

submerged canopy. There is a roughness sub-layer right above the vegetation canopy and a stress-driven region right below it. Both of them make the so-called mixing-layer, within which the water velocity decreases, mainly due to turbulent stress. Below this mixing-layer, the water flow is driven by pressure gradients.

These authors state that the submerged vegetation manifests itself as additional bed roughness.

Bradley and Houser, 2009 discuss that, in low energy conditions, seagrass is swaying over the wave cycle. According to these authors, the ability of seagrass to attenuate wave energy decreases as incident wave heights increase, because the seagrass becomes extended in the direction of flow and rigid, for a longer part of the wave cycle. Moreover, Bradley and Houser, 2009 suggest the use of an equivalent roughness to describe wave attenuation due to a canopy.

Infantes et al., 2012 also mention equivalent roughness, that accounts for the effects of both the sandy bed and the vegetation meadow, and is likely to be a function of the meadow geometry.

In their study on an area in the southeastern part of the coast of England, Möller and Spencer, 2002 remark a seasonal pattern in the wave energy attenuation (highest in September – November and lowest in March – July), that is to be linked to the cycle of seasonal vegetation growth. Möller, 2006 states that the wave attenuation by saltmarsh vegetation is effective up to a threshold value. In a later study, Möller et al., 2014 estimate that up to 60% of observed wave reduction is attributed to vegetation, even when high waves progressively flatten and break vegetation stems, thus reducing dissipation.

Newell and Koch, 2004 performed a study on seagrass on an area located on the North American mid-Atlantic coast. This study states that significant wave reduction, especially during storm events, can be achieved with high vegetation densities, around a critical value of 1000 stems/m^2. Feagin et al., 2011 have determined the biophysical parameters of three salt marsh plant species, in order to improve the implementation of vegetation in numerical models.

Price et al., 1968; Asano et al., 1993; Blackmar et al., 2014 investigated waves passing over vegetation simulated by polypropylene fibres. Fonseca et al., 1982 published a study on the influence of seagrass on current flow. Fonseca and Cahalan, 1992 studied wave energy reduction by four types of seagrass, based on experiments in a wave flume, and stated that only leaf length was found to have a significant contribution to reduction in wave energy. Fonseca and Koehl, 2006 analysed the behavior of artificial seagrass constructed to resemble *Zostera marina* beds and concluded that bed width significantly influences flow behavior and turbulence intensity within the canopy.

Larkum et al., 2006 provide a detailed review of the main aspects concerning various types of seagrasses and stress that flume experiments proved that reduction in wave energy has also been observed at higher depth (5 to 15 m deep), where the plants occupied only a small portion of the water column.

Ma et al., 2012, 2013 developed a non-hydrostatic model for simulating wave refraction, diffraction, shoaling, breaking and landslide-generated tsunami in finite water depth, in order to study turbulence, wave damping and nearshore circulation induced by aquatic vegetation. Finally, Ma et al., 2015 implemented a cohesive sediment transport module into the non-hydrostatic model.

The wave energy dissipated by vegetation is estimated in terms of drag coefficients (Kobayashi et al., 1993; Mendez et al., 1999; Mendez and Losada, 2004; Myrhaug et al., 2009; Sánchez-González et al., 2011; Infantes et al., 2012; Ma et al., 2013, 2015; Koftis et al., 2013; Pinsky et al., 2013; Losada et al., 2016; Luhar et al., 2017; Foster-Martinez et al., 2018; He et al., 2019), by applying Dalrymple's rigid model (Dalrymple et al., 1984).

The effects of *Posidonia oceanica* meadows on the wave height have been studied by various authors, using wave flume experiments. We can mention, among others, the works of Ota et al., 2004; Manca et al., 2010, 2012; Sánchez-González et al., 2011; Koftis et al., 2013. Experiments have indicated that *Posidonia oceanica* meadows are effective at reducing wave energy, especially under low wave energy conditions and small wave amplitudes (Manca et al., 2012).

Ondiviela et al., 2014 discuss the optimal conditions for enhancing protection by seagrass, such as shallow waters, low wave energy environments, with high interaction surface. They also compare native European seagrass species, among them *Zostera marina* and *Zostera noltei* (or *Zostera noltii*).

Sierra et al., 2017 analyse the efficiency of *Zostera marina* meadow to attenuate the impact of Sea Level Rise on breakwater overtopping in two harbours on the Catalan coast through numerical modelling.

Short et al., 2010 show that the seagrass species *Zostera noltei*, which is catalogued as of 'Least Concern' on the IUCN Red List of Threatened Species, is present on most of the Europe coast, from 1 to 10 m deep.

According to the site http://maps.iucnredlist.org, *Zostera noltei* is spread in the eastern Atlantic as well as the Baltic, Mediterranean, Black, Caspian and Aral Seas, and also in western Africa, in Mauritania and in the Canary and Cape Verde Islands (Fig. 1).

Paul and Amos, 2011 have carried out a study on a *Zostera noltei* meadow, located on the north coast of the Isle of Wight and concluded that a minimum shoot density is necessary to initiate wave attenuation. Ganthy et al., 2013a have carried out a study on the influence of *Zostera noltei* meadows on sediment dynamics on a part of the Atlantic coast, in the southwest of France. In a later stage, flume experiments have been conducted in order to develop a 3D numerical model to simulate impacts of *Zostera noltei* beds on hydrodynamics (Ganthy et al., 2013b;

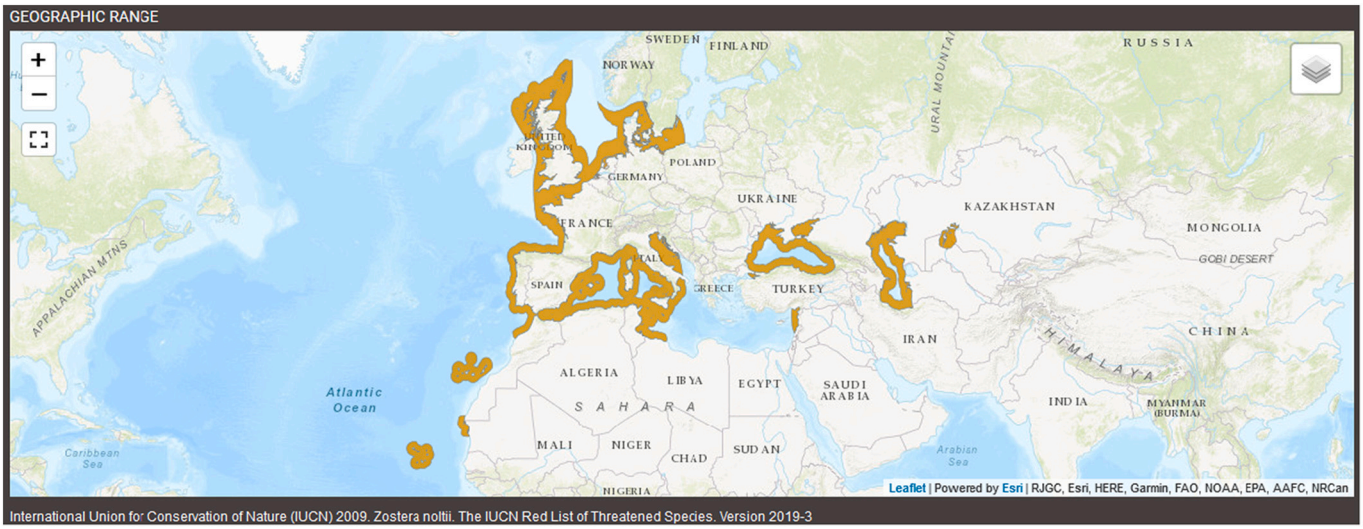

Fig. 1. Spreading of the *Zostera noltei* species (http://maps.iucnredlist.org/map.html?id=153538).

Kombiadou et al., 2014). The results have shown that velocity attenuation was more efficient for flexible species, such as *Zostera noltei,* than for rigid vegetation. In a later study based on flume experiments, Ganthy et al., 2015 stated that the efficiency of sediment trapping by the *Zostera noltei* canopies was found to be density-dependent and seasonally variable, with highest net trapping at high density values.

The presence of *Zostera noltei* on the southern Romanian coast is mentioned in the area of the Mangalia town (Marin et al., 2013; Niță et al., 2014; Surugiu, 2008; Surugiu et al., 2021). Surugiu, 2008 also provides a description of this species, with stem heights up to 20 cm. Niță et al., 2014 mention the depth of 3 m in the area of Mangalia, but Surugiu, 2008 states that, in the Black Sea, this species can be found down to 8–10 m deep, in sheltered areas.

This species is currently regenerating along the Romanian coast and its presence is associated to a good environmental state (Marin et al., 2013). Niță et al., 2014 analysed the possibility for transplantation of *Zostera noltei*, in the area north of Mangalia, in order to regenerate the specific aquatic vegetation along the Romanian coast, as it has an important ecological value for the shallow marine ecosystems.

These authors explain that, in the past, *Zostera noltei* formed wide underwater meadows in several zones along the southern Romanian coast, including the zone close to Mangalia, where our study area is located. They state that *Zostera noltei* has undergone a drastic decline as a follow-up of uncontrolled dredging and water transparency reduction, caused by large amounts of suspensions resulting from various anthropogenic activities. The same information can be found in Surugiu, 2008; Surugiu et al., 2021.

Niță et al., 2014 also stress the fact that the two analysed species are undergoing a regeneration process along the Romanian coast. Moreover, they state that *Zostera noltei* forms meadows in the southern part of the Romanian coast, in the area of Mangalia.

In their study, the area selected for harvesting *Zostera noltei* is in the exterior zone of the northern breakwater of the Mangalia Shipyard, while the translocation site was selected in the northern part of the Olimp resort, that is north of our study area. Both selected areas are at depth around 3 m.

The key-species samples were transplanted successfully from the harvesting locations to the new selected sites. The monitoring performed has revealed the stability of the relocated samples.

Considering this information, we are confident that planting *Zostera noltei* in our study area is also feasible.

Nevertheless, there is no information available on *Zostera noltei* stem density along the Romanian Black Sea coast.

Most of the above-mentioned works focus on vegetation as a key element of the local ecosystem, without analysing the effectiveness in protecting the coast in a representative wave climate.

This work aims to address this challenge, by using numerical modelling of wave damping due to vegetation, included in a subroutine of the SWAN (Simulating WAves Nearshore) spectral wave-model (Booij et al., 1999).

For the southern Romanian coast, the protection needs have been traditionally solved by classic means, such as hard coastal defenses.

In a previous study on protection and rehabilitation of the southern Romanian coast (JICA, 2008), the barrier beach between Venus and Saturn is listed among the ones that do not need urgent measures, as it is wide enough. In the Master Plan for Protection and rehabilitation of the coastal zone of Romania (HALCROW UK et al., 2012), this barrier beach is listed among the ones with recommended additional soft measures, such as nature-based solutions, to reduce the risk of erosion.

A preliminary attempt to test the effectiveness of soft measures on the southern Romanian coast has been performed by the same authors and can be found in Monclús i Bori et al., 2019.

The present work comprises the full analysis of the proposed green solution, using the waves from all the directions that may have an impact on the barrier beach between Venus and Saturn.

Several numerical simulations have been performed, using a wave distribution model, first in the absence of the vegetation meadow, then adding it to our modelled domain, for present-day wave climate conditions (Lin-Ye et al., 2018).

The aim of this paper is to evaluate whether planting seagrass could be considered as an appropriate measure to protect southern Romanian coast beaches against erosion. This study contemplates reduction in coastal erosion, as directly proportional to wave attenuation due to vegetation. Wave damping has been assessed with a spectral wave model that simulates a hypothetical *Zostera noltei* meadow placed in front of a protected site.

2. Study area

Our study focuses on a barrier beach from the southern Romanian coast (Fig. 2), in front of a protected Natura 2000 site, known as 'Balta Mangalia' (Mangalia Marsh), which is a 4th category nature reserve according to IUCN (*International Union for Conservation of Nature* and Natural Resources) since January 2005.

The barrier beach is located northwards to Mangalia town, between the geographic coordinates 43.830–43.841°N and 28.589–28.592°E. This low-lying beach extends on about 1.3 km along the coast, between the Venus and Saturn resorts (Fig. 1). Its width goes roughly from 20 m

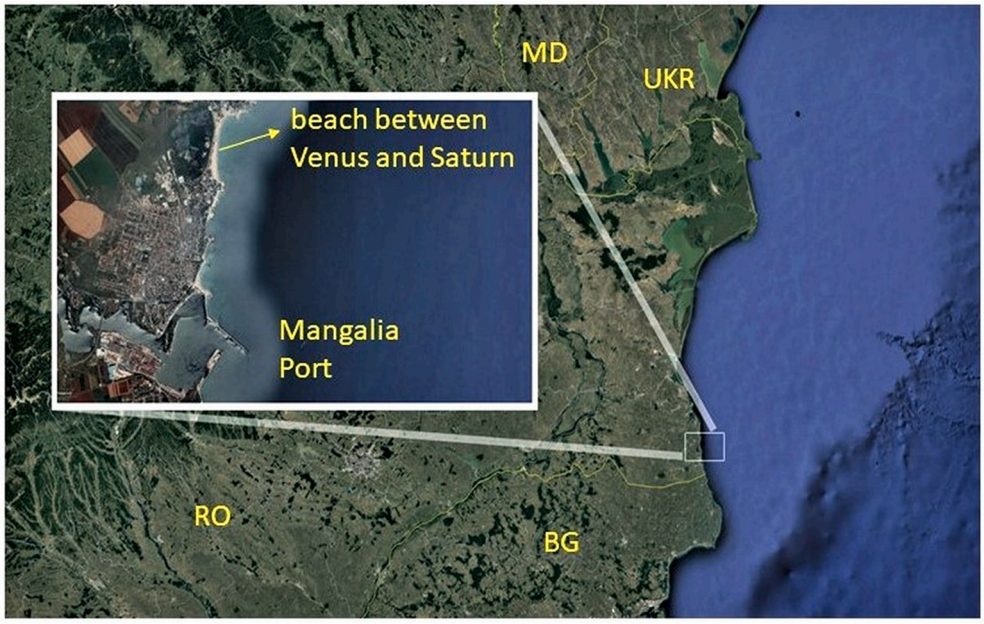

Fig. 2. Study area between the Venus and Saturn resorts, north of Mangalia, Romania, western Black Sea coast.

at the southernmost end to 180 m locally. The beach elevation is between 1.2 m and 0.2 m in the vicinity of the shoreline.

There are no coastal defenses along this beach. Therefore, it is considered to be at high risk due to erosion in case of extreme storm events. There is an estimated erosion trend between −1 and −3 m/year, according to the Master Plan for the Romanian Coast (HALCROW UK et al., 2012).

The barrier beach between Venus and Saturn consists of mainly medium to coarse sand. The mean diameter (D50) of beach sediments increases north to south, reaching 0.58 mm in the area south of Mangalia area (HALCROW UK et al., 2012). Constantinescu and Giosan, 2017 state that this D50 variation reflects the change in sediment source. The available information (HALCROW UK et al., 2012) provides the representative mean grain size value of 0.48 mm for the beach sediments north of Mangalia, including the beach between Venus and Saturn.

In this area there are few built assets and a main road that separates the beach from the Balta Mangalia area. Nevertheless, it is attractive for tourists, especially in its northern and southern parts, where the beach is wider and close to hotels in Venus and Saturn resorts.

The average offshore significant wave height along the whole Romanian coast increases from north (0.85 m) to south (0.95 m). The severest storms are from the northern sector and occur during winter

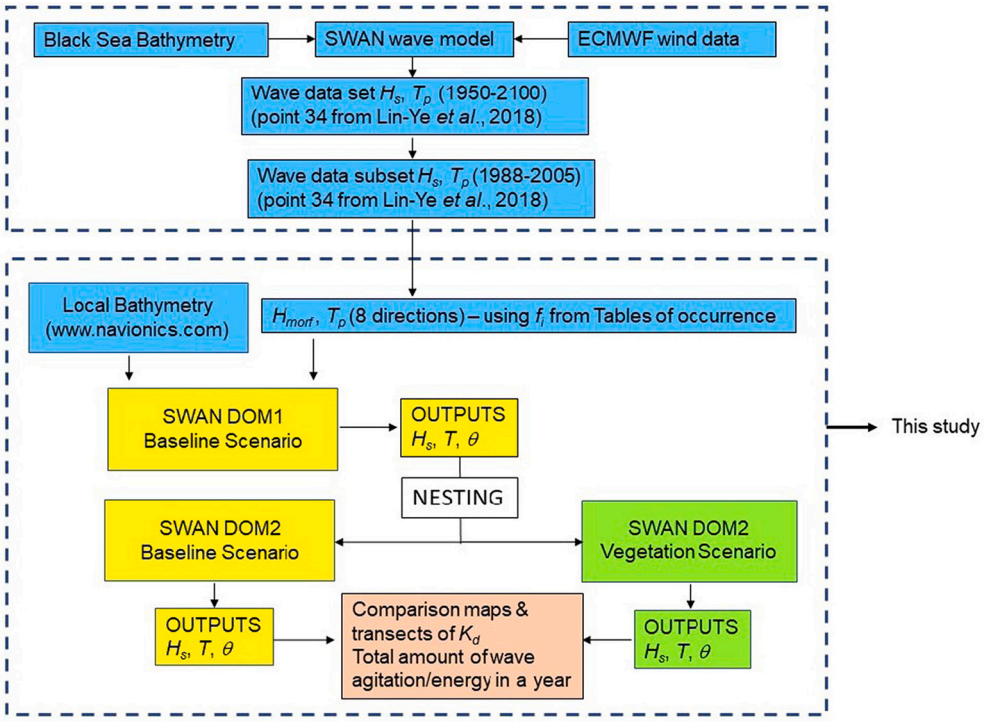

Fig. 3. Flowchart illustrating the methodology used.

periods (November to March). The maximum significant offshore wave heights may exceed 6 m and are associated with peak wave periods over 13 s (HALCROW UK et al., 2012).

According to JICA, 2008, the Mean Water Level records are between −0.304 m (January 1992) and 0.902 m (February 1979) and tide is very low, in the order of 0.05 m. The tide in the Black Sea has an average period of 12 h 25′ and amplitudes of only 0.07–0.11 m (Sorokin, 1982; Bondar, 1989; Panin, 2005).

The Master Plan for the Romanian Coast (HALCROW UK et al., 2012) mentions the barrier beach between Venus and Saturn among the ones where beach recharge and soft measures represent the most appropriate policy, in order to reduce the erosion risk.

3. Methodology

In this contribution, we have followed the methodology in the flowchart shown in Fig. 3, in order to analyse the effect of the *Zostera noltei* meadow, using numerical nested simulations.

3.1. Input data

The input data consists of two main types (Fig. 3): (i) bathymetry data and (ii) wave data.

In order to build the numerical model, the bathymetry data have been derived from existing multiple charts (www.navionics.com). Our study domain covers a 28 km wide alongshore strip and the bathymetry values are up to 50 m deep.

The wave data used in our work is available from a previous study, performed by Lin-Ye et al., 2018, that characterized the extreme wave climate for the northwestern Black Sea using a hybrid strategy for two climate change scenarios, the Representative Concentration Pathways (RCPs) 4.5 and 8.5 (Church et al., 2013; Stocker et al., 2013). The authors used as input the wind fields obtained by the ALADIN model (Colin et al., 2010; Farda et al., 2010; Herrmann et al., 2011) and downloaded from the Mediterranean Coordinated Regional Downscaling Experiment (Med-CORDEX) initiative (Ruti et al., 2016). These winds fields were used as inputs for the SWAN spectral wave model run in a non-stationary mode. The computational domain spanned the whole Black Sea with a regular grid of 9 km × 9 km. The wave outputs were saved hourly at a subset of 34 computational nodes of the northwestern Black Sea. Lin-Ye et al., 2018 used the above-mentioned SWAN outputs in order to produce wave-climate projections for the northwestern part of the Black Sea. The validation dataset, in both emission scenarios, was the ERA-Interim reanalysis data set (Dee et al., 2011), provided by the European Centre for Medium Weather Forecast (ECMWF), covering 38 years, from 1979 to 2016.

The data set used in our study is from the node 34, available from Lin-Ye et al., 2018 (Figs. 3, 4). This node is the one located closest to the southern Romanian coast. The original wave data set covers 150 years. For this work, we decided it would be reasonable to use a subset of 18 years, featuring present climate, from 1988 to 2005. During this period the wind fields coincide for both RCP scenarios. According to Puertos del Estado, 1994, a minimum period of 3 years of data is required to characterize the wave conditions.

Also, note that only the waves that would reach the coast have been considered in this study. Such waves are coming from the NNE to S directions.

For every analysed direction, several wave height intervals, in 0.5 m bins, and wave period intervals, in 2 s bins, have been established. Then, wave height values have been counted for each of these intervals. Finally, the frequency of occurrence has been computed for each case, by dividing the number of above-mentioned values by the total number of observations. This information is reported in Appendix A – Tables A.1 to A.8, corresponding to the 8 wave directions considered: NNE, NE, ENE, E, ESE, SE, SSE, and S.

Based on the Tables A.1 to A.8, the wave roses for the significant wave heights and associated wave periods have been represented (Fig. 5).

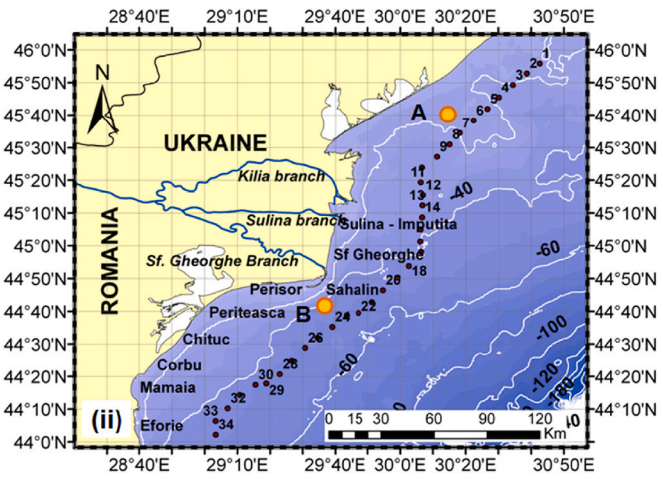

Fig. 4. Nodes of the statistical model of the reanalysis in the northwestern Black Sea (from Lin-Ye et al., *2018*).

The study is focused on the effects of a seagrass meadow in a typical mean wave climate year, which is represented by calms, mild energy conditions and storms. For this reason, a synthetic wave climate is constructed by means of a root mean squared frequency weighted estimation, H_{morf}, for each wave period.

The H_{morf} is defined as:

$$H_{morf} = \sqrt{\left(\sum H_i^2 f_i\right) \Big/ \left(\sum f_i\right)} \text{ [L]}, \quad (1)$$

where: i is the number of a registered wave height between certain limits, H_i is the wave height and f_i is its frequency of occurrence.

The values of H_i and f_i can be found in Appendix A – Tables A.1 to A.8. The H_i values have been considered in the middle of every wave height incremental interval. So, for the interval 0–0.5 m, the corresponding H_i value is 0.25 m; for the interval 0.5–1 m, the corresponding H_i value is 0.75 m. The results of the H_{morf} calculations are reported in Table 2.

Similar wave climate simplifications are common practices in coastal engineering (U.S. Army Corps of Engineers, 2002).

The purpose of these calculations was to establish the wave height that synthesizes the wave information, for every direction analysed. The H_{morf} values and the associated wave periods have been used in the setup of the SWAN simulations.

3.2. Seagrass characteristics

In what concerns the stem density, various authors provide differing values.

Stem densities in laboratory studies may reach high values. The purpose of such experiments is to assess the mechanisms of controlling the wave transformation and the interdependence of specific seagrass features. In their experimental study, Fonseca and Koehl, 2006 mention a density of the artificial seagrass patches of 1000 stems/m^2. Ciraolo et al., 2006 mention densities of 500 and 1000 stems/m^2 for their flume experiments to investigate the flow resistance of *Posidonia oceanica*. Sánchez-González et al., 2011 discuss flume experiments to investigate the effect of *Posidonia oceanica* meadows on wave height and mention stem densities starting from 400 stems/m^2, but also reaching high values of 40,000 stems/m^2.

Manca et al., 2010, 2012 also present results of wave flume experiments and mention stem densities of 180 and 360 stems/m^2 of artificial *Posidonia oceanica*. In their study, also based on wave flume experiments with artificial *Posidonia oceanica*, Koftis et al., 2013 mention stem

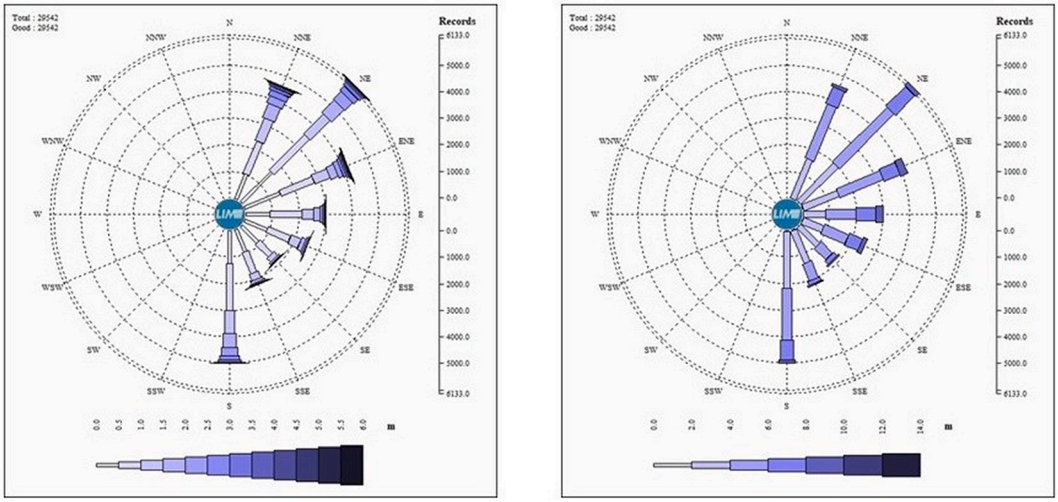

Fig. 5. Wave rose of the significant wave heights (a) and wave periods (b), for the analysed directions. (For interpretation of the references to colour in this figure legend, the reader is referred to the web version of this article.) (For interpretation of the references to colour in this figure legend, the reader is referred to the web version of this article.)

Table 2
Computed H_{morf} and associated mean wave periods used in the setup of simulations.

Wave Direction	H_{morf} (m)	Mean Wave Period T (s)
1-NNE	1.36	5
1-NNE	2.76	7
1-NNE	3.49	9
2-NE	1.17	5
2-NE	2.32	7
2-NE	3.53	9
3-ENE	1.02	5
3-ENE	1.92	7
3-ENE	2.97	9
4-E	0.92	5
4-E	1.37	7
4-E	2.24	9
5-ESE	0.88	5
5-ESE	1.40	7
5-ESE	2.13	9
6-SE	1.00	5
6-SE	1.29	7
6-SE	1.90	9
7-SSE	1.14	5
7-SSE	1.91	7
7-SSE	1.68	9
8-S	1.27	5
8-S	2.21	7
8-S	2.75	9

densities between <150 (denoted as 'sparse') and higher than 700 (denoted as 'dense'). Ros et al., 2014 discuss experiments with densities ranging between 128 and 1280 stems/m^2. Luhar et al., 2017 discuss experiments on a meadow to mimic *Zostera marina* seagrass, with density of 1800 stems/m^2. The density of 1000 stems/m^2 can also be found in some works based on field data, such as the ones carried out by Newell and Koch, 2004; Chen et al., 2007; Koch et al., 2009.

Fraschetti et al., 2013 have carried out a study on *Posidonia oceanica* meadows in a Mediterranean Marine Protected Area in the southeastern part of Italy. They provide density values between 100 and 750 stems/m^2 for this seagrass species. In their study area, located on the northeast coast of Spain, Granata et al., 2001 mention stem densities of *Posidonia oceanica* that may reach around 400 stems/m^2. In their studies on the *Posidonia oceanica* meadow located along the northeast coast of Mallorca, Infantes et al., 2012 and Luhar et al., 2013 mention measured densities around 600 stems/m^2.

In their study concerning proposed green measures for two harbours located on the Catalan coast, Sierra et al., 2017 have studied the effect of a *Zostera marina* meadow, using numerical modelling and considering various values for the vegetation density of 50 stems/m^2 and 100 stems/m^2.

Some authors state that *Zostera noltei* may reach very high densities in the Mediterranean area, over 20,000 stems/m^2 (Curiel et al., 1996; Ondiviela et al., 2014). For the *Zostera noltei* meadow in their study area on the Isle of Wight, Paul and Amos, 2011 discuss stem density values around 4600 stems/m^2 in summer and 600 stems/m^2 in winter. For the *Zostera noltei* meadow in the area of Arcachon Bay, France, Kombiadou et al., 2014 mentions low densities of 4000 to 9000 stems/m^2 and high densities of 11,000 to 22,000 stems/m^2.

In what concerns the Black Sea area, stem densities are usually lower than in the Mediterranean area. There are areas in Crimea where *Zostera noltei* can reach high densities, exceeding 3000–4000 stems/m^2 during summer, such as Kerch Bay, Kerch Strait (Milchakova and Phillips, 2003). However, Phillips et al., 2006 report values around 100 stems/m^2 for *Zostera noltei* in the area of Sevastopol Bay and refer to its presence as 'sporadic', after collecting samples in April 2002, September 2002 and January 2003. Holmer et al., 2016 also provide higher density values for *Zostera noltei* in the area of Sozopol Bay, Bulgaria, around 1000 stems/m^2.

In a recent study on the distribution of *Zostera* seagrass meadows along the Bulgarian coast, Berov et al., 2022 mention stem densities for *Zostera noltei* between 750 and 2250 stems/m^2 and stem heights between 20 and 40 cm in the area of Burgas Bay. These authors state that the most extensive seagrass meadows in the Black Sea are found in its north-western part and along the Crimean coast (Ukraine and Russia), where they grow in large bays and gulfs, coastal lagoons and river mouths and deltas. Starting with the 1970s, due to pollution and eutrophication, seagrasses have declined drastically in abundance in the area of the Romanian coast and in other parts of the Black Sea (Surugiu, 2008; Surugiu et al., 2021). Berov et al., 2022 discuss that the Romanian Black Sea coast is relatively open and exposed to currents and winter storms, offering few suitable habitats for seagrasses. They also stress that the Romanian seagrass meadows declined significantly due to poor

water quality in the 1980s and small ones are currently reported near Mangalia and Vama Veche.

Niță et al., 2014 state that *Zostera noltei* has undergone a drastic decline along the Romanian coast, due to uncontrolled dredging and water transparency reduction but, in recent years, they are undergoing a regeneration trend. They discuss that *Zostera noltei* can be affected by the presence of suspensions, by limitation of light penetration in water, leading to transparency reduction, as well as by siltation processes. These authors state that a sheltered area with high water transparency, not being under the direct influence of waves and currents, favors the development of this species.

Taking this information into account, we have chosen a stem density value of 100 stems/m^2 for our simulations. A higher density value would be unrealistic for this location, as it is not sheltered, unlike the areas of Sevastopol Bay and Burgas Bay.

Nevertheless, under the specific conditions of our study area, the density of 100 stems/m^2 characterizes a well-developed *Zostera noltei* meadow.

3.3. The wave model and simulations setup

The evaluation of the effect of the seagrass meadow has been done by means of the numerical model SWAN, Simulating WAves Nearshore (Booij et al., 1999). The SWAN model is a third generation, phase-averaged, open-source numerical model based on a Eulerian formulation of the discrete spectral balance of action density, that accounts for refractive propagation over arbitrary bathymetry and current fields (Booij et al., 1999). The spectral energy balance models can be extended to shallow water, accounting for the specific phenomena occurring when waves approach the coastline - refraction, shoaling and diffraction (Holthuijsen, 2007).

The SWAN model solves the action balance equation with the associated source and sink terms, without a priori no restriction with the wave spectra. For this specific case study, the nearshore wave propagation terms have been activated, whereas the wave generation (more suited to deep waters) has been de-activated.

The wave dissipation energy has been modelled through three processes: bottom friction (Madsen et al., 1988), wave depth-induced breaking (Battjes and Janssen, 1978) and dissipation by vegetation (Suzuki et al., 2012). This last vegetation module, has been used in recent works for including the influence of vegetation on wave fields (McIvor et al., 2012; Vuik et al., 2016; Van Rooijen et al., 2016). The module consists of a parametrization of wave energy proportional to specific submerged vegetation features: stem density, stem average height, canopy width and the drag coefficient. This drag coefficient is estimated with the method proposed by Myrhaug and Holmedal, 2011.

A nesting strategy was established, in order to obtain a detailed hydrodynamic information in the area. Two domains have been defined with different extents and resolutions (Fig. 6).

The large domain, DOM1, covers 476 km^2 and reaches 50 m deep. The smaller domain, DOM2, that includes the seagrass field, covers 49 km^2 and goes roughly until 35 m deep.

Both domains have been generated using the Kriging method. They consist in regular meshes with equal grid spacing in the x and y directions (i.e. 80 m in DOM1 and 15 m in DOM2).

The spatial extent of the proposed vegetation mask has been established so that it would be between 2 and 6 m deep, roughly covering 1 km^2 and extending about 1.5 km alongshore, with a maximum width of 650 m (Fig. 7). The stem height and section area values have been established according to the information on *Zostera noltei* provided by Surugiu, 2008 and Short et al., 2010. Thus, the stem height has been considered 20 cm, a maximum value, according to Surugiu, 2008, characteristic for a well-developed meadow.

3.4. Simulation scenarios

A Baseline Scenario and a Vegetation Scenario have been defined for every one of the 8 wave directions considered. The Baseline Scenario consists in applying the wave forcing on the represented domain as it is. The Vegetation Scenario consists in adding a vegetation mask to the domain, which is characterized by spatial extent, stem height, stem width, stem density, as well as the drag coefficient (Myrhaug and Holmedal, 2011), which depends on the wave height and period, the depth where the vegetation is located, and the stem height. Finally, the calculated drag coefficient has the average value of 0.095, for all the wave conditions reported in Table 2.

The SWAN model has been run with the Baseline Scenario first in the absence of vegetation, on DOM1. The output has been stored in points around DOM2 and used as the new boundary condition. To reduce the computational time, the Baseline Scenario and the Vegetation Scenario have been run again on DOM2 and the results have been compared (Fig. 3). Such simulations have been run for every wave forcing reported in Table 2.

Thus, a total number of 72 simulations (Baseline Scenario on DOM1

Fig. 6. The two domains of the nesting.

Fig. 7. Points along three transects (north, center, south) through the vegetation meadow; the green line marks the vegetation meadow contour. (For interpretation of the references to colour in this figure legend, the reader is referred to the web version of this article.) (For interpretation of the references to colour in this figure legend, the reader is referred to the web version of this article.)

and DOM2 + Vegetation Scenario on DOM2, for 24 different wave forcings) have been performed.

3.5. Attenuation coefficient, wave agitation and wave energy

The wave attenuation, agitation and energy are shown at 3 representative transects covering the area of study (Fig. 7). A similar approach has been used by la Hausse de Lalouvière et al., 2020. The north and south transects, located at the boundaries, include the shadow effects that coastal structures can induce, whereas the center transect is a good example of the main possible wave directions: normal and oblique to the beach.

Each transect has been defined by 10 points: N1 to N10 along the north transect, C1 to C10 along the center transect, and S1 to S10 along the south transect.

The results of the Baseline and Vegetation scenarios in all the points along the three transects are shown in Appendix B, Tables B.1 to B.3.

For every wave direction, attenuation coefficients have also been calculated, as following:

$$K_d = H_V/H_B, \quad (2)$$

where:

H_B is the wave height for the Baseline scenario;

H_V is the wave height for the Vegetation scenario.

Many storms would impact our study area during a year, basically from all the analysed directions. We can estimate the effect of all these storms during a year, by summing up the results of all the runs, weighted by their corresponding frequencies of occurrence.

Wave Agitation (*WA*) during a year, on our study area, is assessed taking into account the frequency of the wave directions that would impact the coast in the present and future conditions, as previously discussed in the work of Casas-Prat and Sierra, 2010.

Thus, *WA* can be expressed as:

$$WA_B = \sum_i H_{Bi} f_i \ [\mathrm{L}] \text{ for the Baseline scenarios and} \quad (3a)$$

$$WA_V = \sum_i H_{Vi} f_i \ [\mathrm{L}] \text{ for the Vegetation scenarios} \quad (3b)$$

In the formulae above, the f_i values are the frequencies of occurrence, taken from the Tables of occurrence A.1 to A.8 (Appendix A); H_{Bi} are the wave heights for the Baseline scenarios and H_{Vi} are the wave heights for the Vegetation scenarios.

Finally, the *WA* reduction is calculated as:

$$WA_{red} = 100\,(1 - WA_V/WA_B) \ [-] \quad (4)$$

Wave Energy (*WE*) can be expressed starting from the formula for random irregular waves (Holthuijsen, 2007):

$$E = (1/16)\rho g H_s^{\,2} \ \left[\mathrm{M}\cdot\mathrm{T}^{-2}\right] \quad (5)$$

In the formula above, E is the mean wave energy density per unit horizontal area, ρ is the sea water density [$\mathrm{M}\cdot\mathrm{L}^{-3}$], g is the gravitational acceleration [$\mathrm{L}\cdot\mathrm{T}^{-2}$], equal to 9.81 m/s^2, and H_s is the significant wave height [L].

Similarly, the total wave energy density per unit horizontal area (*WE*) during a year can be expressed as following:

$$WE_B = (1/16)\rho g \sum_i H_{Bi}^2 f_i \ \left[\mathrm{M}\cdot\mathrm{T}^{-2}\right] \text{ for the Baseline scenarios} \quad (6a)$$

and

$$WE_V = (1/16)\rho g \sum_i H_{Vi}^2 f_i \ \left[\mathrm{M}\cdot\mathrm{T}^{-2}\right] \text{ for the Vegetation scenarios} \quad (6b)$$

For the Black Sea, the water density has been considered 1015 kg/m^3, based on the information available in Yankovsky et al., 2004.

Finally, the *WE* density reduction is calculated as:

$$WE_{red} = 100\,(1 - WE_V/WE_B) \ [-] \quad (7)$$

4. Results

The calculated wave height differences between the Baseline and the Vegetation Scenarios were plotted for every direction. The plots have

differing color scales because the differences in wave heights are too low to be visible at specific cases. So, for each plot, the color scale is set to correspond to the minimum and maximum values of the calculated wave height differences. The distributions of the calculated wave height difference between the Baseline and the Vegetation scenarios, for two wave directions, are shown on Fig. 8a and b. The wave heights and wave periods values are the ones from Table 2, for NE and SSE.

The significant wave height variation from offshore to inshore along the three transects, for the mean wave period of 9 s, is shown on Fig. 9, for waves from NE, and on Fig. 10, for waves from SSE. Figs. 9 and 10 indicate the attenuation induced by the seagrass, for both wave directions and the highest period considered that can be associated with the extreme storms. The waves from SSE are more attenuated than the ones from NE, because they travel more through the vegetation meadow.

4.1. Attenuation coefficient K_d

The attenuation coefficient K_d values are reported in Appendix B, Tables B.1 to B.3. There are points along each transect where the wave height provided by the SWAN model is identical for the Baseline and Vegetation scenarios, so the calculated K_d values are 1. There are other points where the wave heights for the Vegetation scenario are slightly higher than the ones for the Baseline scenario, for specific wave conditions. Thus, we have reported no attenuation when the ratio between the wave height for the Vegetation scenario and the wave height for the Baseline scenario is at least 1.01 (Tables B.1 to B.3).

Figs. 11 to 13 show the attenuation coefficient K_d versus cross-shore distance along the three transects, for the considered mean wave periods. A decreasing trend in the K_d values can be noticed in most cases, until 250–300 m from the shoreline, followed by an increasing trend with the distance.

On the north transect, the highest attenuation for the waves with mean periods of 5 s and 7 s occurs after crossing the vegetation meadow, at 230 m from the shoreline (Fig. 11a and b). Highest attenuation for the waves with the mean period of 9 s occurs within the vegetation meadow, at about 320 m from the shoreline (Fig. 11c). The waves that are most attenuated are from S and SSE with mean period of 5 s (Fig. 11a), from NE with mean period of 7 s (Fig. 11b), and from E with mean period of 9 s (Fig. 11c). High frequencies of occurrence are associated to the waves from SSE and S with mean period of 5 s (Table 2 and Tables A.7 and A.8), as well as to the ones from NE with mean period of 7 s (Table 2 and Table A.2).

On the central transect, the highest attenuation for the waves with mean periods of 5 s, from NE and ENE, occurs after crossing the vegetation meadow, at over 150 m from the shoreline (Fig. 12a). The highest attenuation for the waves from E, with the mean period of 7 s occurs at the edge of the vegetation meadow, at about 250 m from the shoreline (Fig. 12b). For the mean period of 9 s, the highest attenuation occurs at the shoreline, for the waves from S, and at 250 from the shoreline, for the waves from SSE (Fig. 12c). The waves that are most attenuated are from NE and ENE with mean period of 5 s (Fig. 12a), which show high frequencies of occurrence (Table 2, and Tables A.2 and A.3). The waves from E with mean period of 7 s show high frequency of occurrence as well (Table 2 and Table A.4). The waves from SSE and S with mean periods of 9 s (Fig. 12b and c) do not show high frequencies of occurrence (Table 2 and Tables A.7 and A.8) but travel more through the vegetation meadow.

On the south transect, the highest attenuation for the waves with mean periods of 5 s and 7 s occurs within the vegetation meadow, at 260 m from the shoreline (Fig. 13a and b). There is almost no attenuation for the waves with mean period of 5 s (Fig. 13a). The waves that are most

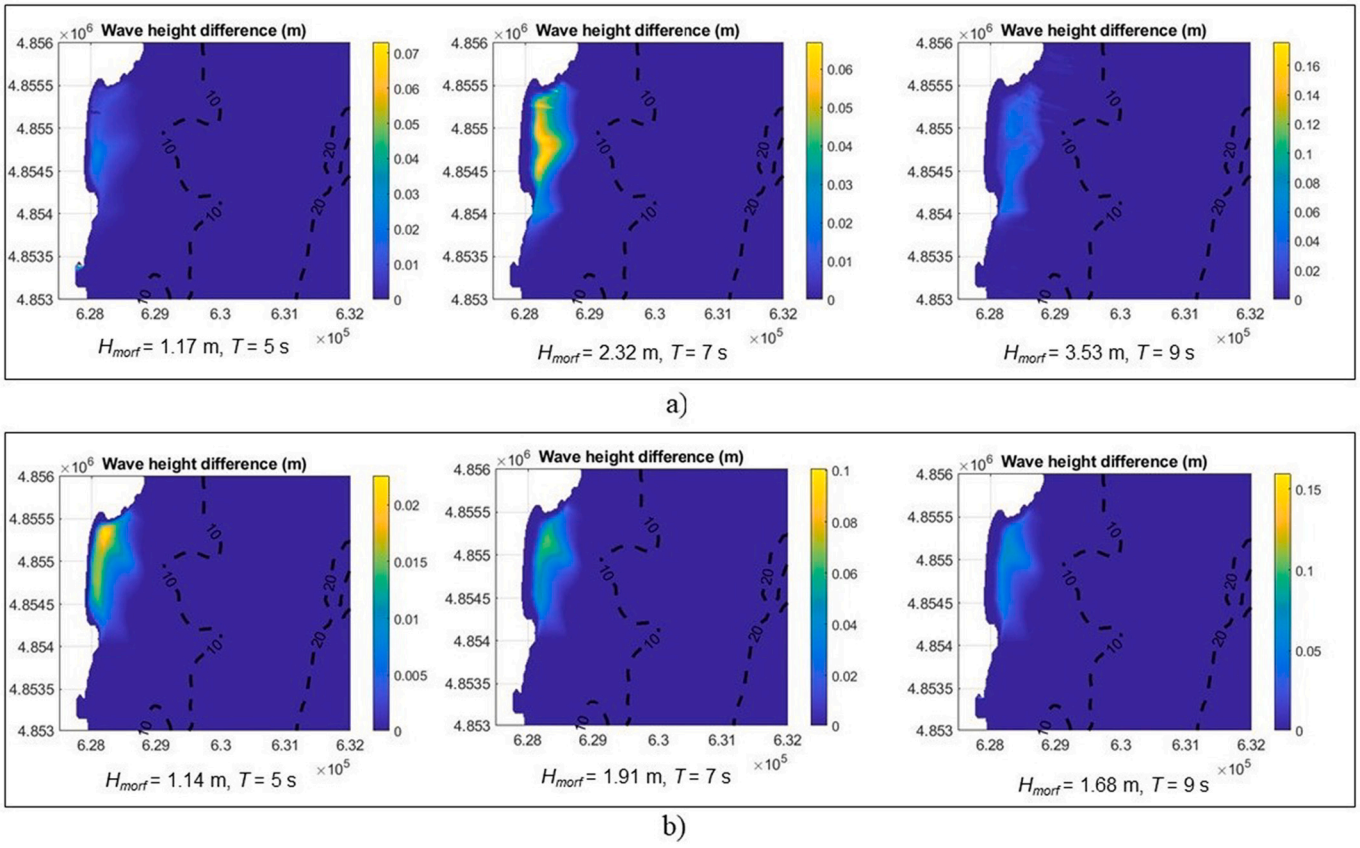

Fig. 8. Distribution of the calculated wave height difference between the Baseline and the Vegetation Scenarios for: a) NE waves; b) SSE waves; the dashed lines represent the bathymetric contours (m).

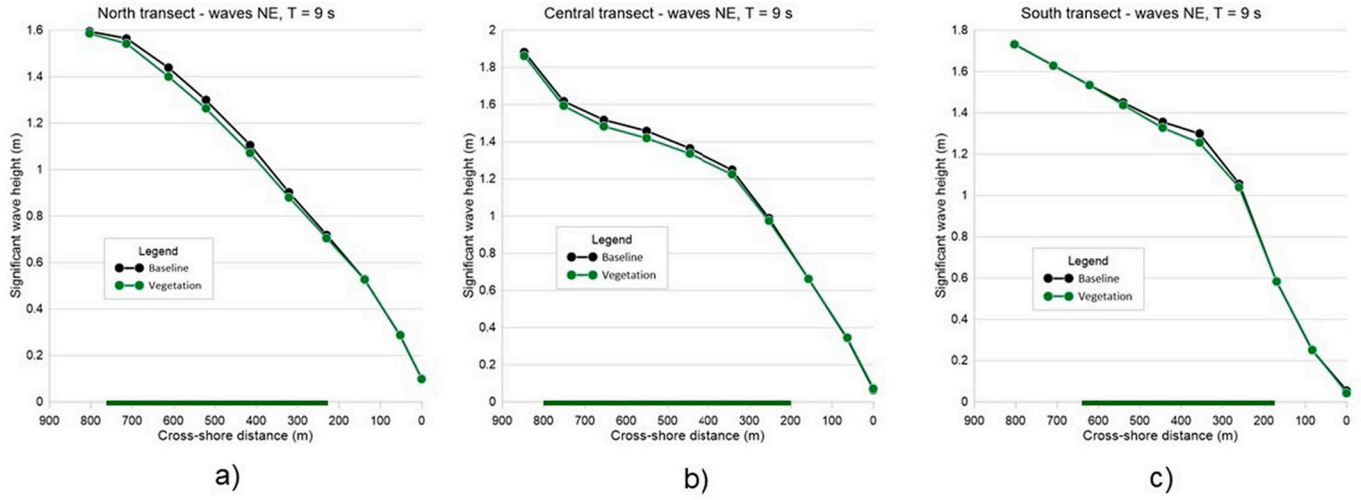

Fig. 9. Distribution of the significant wave height along the three transects, for the waves from NE with mean period of 9 s, for the Baseline and the Vegetation Scenarios; the green line on the horizontal axis marks the extension of the vegetation meadow along the: a) north transect; b) central transect; c) south transect. (For interpretation of the references to colour in this figure legend, the reader is referred to the web version of this article.) (For interpretation of the references to colour in this figure legend, the reader is referred to the web version of this article.)

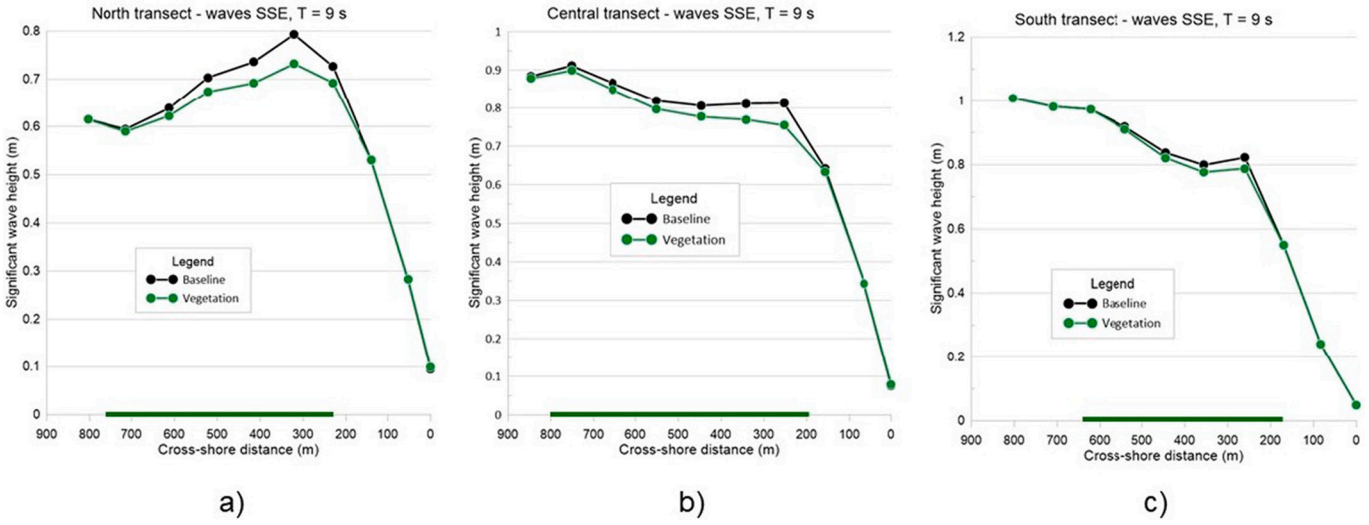

Fig. 10. Distribution of the significant wave height along the three transects, for the waves from SSE with mean period of 9 s, for the Baseline and the Vegetation Scenarios; the green line on the horizontal axis marks the extension of the vegetation meadow along the: a) north transect; b) central transect; c) south transect. (For interpretation of the references to colour in this figure legend, the reader is referred to the web version of this article.) (For interpretation of the references to colour in this figure legend, the reader is referred to the web version of this article.)

attenuated along the south transect are from ENE, with mean period of 7 s (Fig. 13b), and from NE, with mean period of 9 s (Fig. 13c). These waves show high frequencies of occurrence (Table 2 and Tables A.2 and A.3).

Apparently, the highest attenuation by the proposed vegetation meadow (the minimum K_d value of 0.8003) occurs on the south transect at the shoreline, for the waves from NE, with mean period of 9 s (Fig. 13c). But the significant wave heights for the Baseline and Vegetation scenarios are so small, in the order of cm (Table B.3), that they must be neglected. Thus, the minimum K_d value of 0.8003 has no physical meaning.

Therefore, the calculated K_d values can be considered as between 0.9121, on the north transect, for NE waves with mean period of 7 s (Table B.1), and 1 (Tables B.1 to B.3).

Given the shape of the vegetation meadow, the waves from NE, as well as those from S, travel more through it than the ones from the other directions, thus being more attenuated. Moreover, the waves from NE have rather high frequencies of occurrence (Table A.2).

It can be noticed that the waves with periods of 7 s and 9 s are more attenuated than the ones with period of 5 s (Figs. 11 to 13 and Tables B.1 to B.3). This agrees with the experimental results of Lowe et al., 2007 and Koftis et al., 2013, who found that waves with higher period are more attenuated.

Table 3 synthesizes the attenuation results, emphasizing the highest values on every transect. Overall, the highest attenuation by the proposed *Zostera noltei* meadow goes from 2% to 20% locally, on the south transect, at the shoreline, and only for specific conditions - waves from the NE sector, with mean period 9 s.

As stated by Bradley and Houser, 2009, the ability of vegetation to attenuate wave energy is quite variable, depending on the specific combination of hydrodynamic forces and vegetation characteristics. The local bathymetry also has an influence on the hydrodynamics. East of the vegetation meadow there is a small elevated zone, which is included in DOM2, with bathymetry between 4 and 4.5 m deep, while, going more

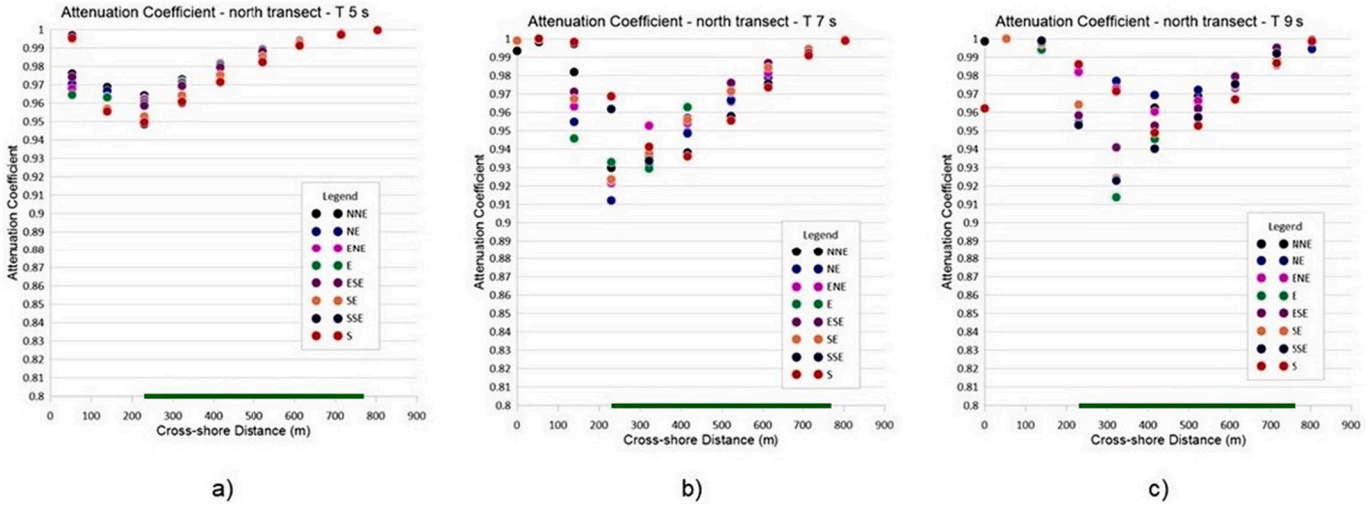

Fig. 11. Attenuation coefficient versus cross-shore distance along the north transect through the vegetation meadow for mean wave periods: a) 5 s; b) 7 s; c) 9 s. The green line on the horizontal axis marks the extent of the vegetation meadow along the transect. (For interpretation of the references to colour in this figure legend, the reader is referred to the web version of this article.) (For interpretation of the references to colour in this figure legend, the reader is referred to the web version of this article.)

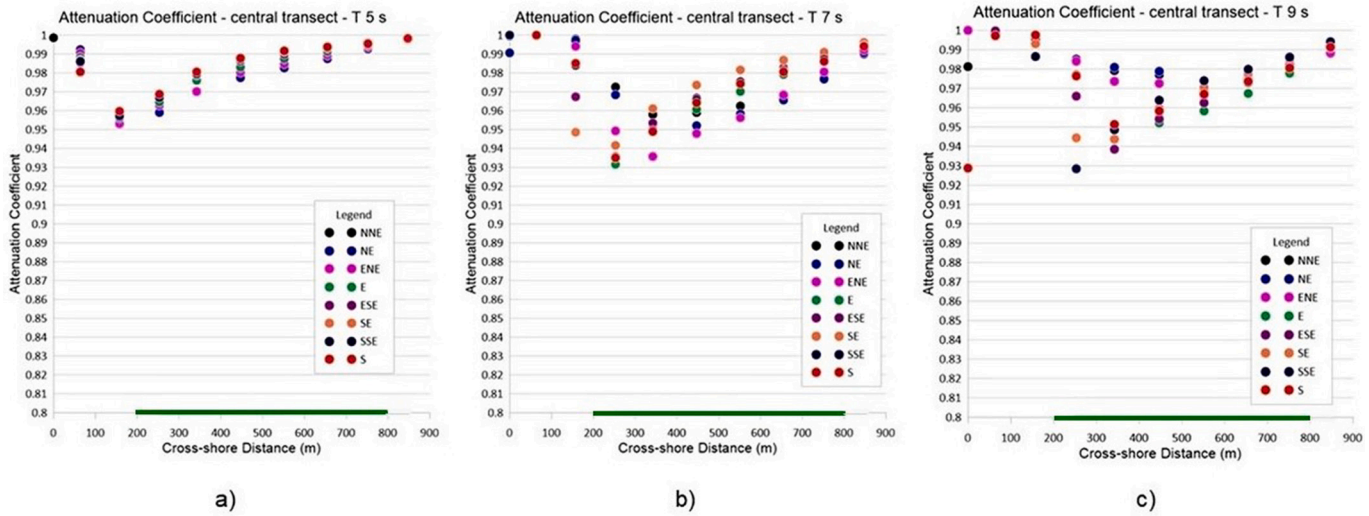

Fig. 12. Attenuation coefficient versus cross-shore distance along the central transect through the vegetation meadow for mean wave periods: a) 5 s; b) 7 s; c) 9 s. The green line on the horizontal axis marks the extent of the vegetation meadow along the transect. (For interpretation of the references to colour in this figure legend, the reader is referred to the web version of this article.) (For interpretation of the references to colour in this figure legend, the reader is referred to the web version of this article.)

towards east, the bathymetry is between 7 and 8 m deep (Monclús i Bori et al., 2019). This elevated zone is an obstacle for the offshore waves, especially the ones coming from the eastern sector.

In their analysis on green measures for two ports on the Catalan coast, Sierra et al., 2017 applied the SWAN model first for baseline scenarios, and then adding a *Zostera marina* meadow to the setup for vegetation scenarios. The stem height was considered 1 m and the density values used were 50 stems/m^2 and 100 stems/m^2. Sierra et al., 2017 obtained decrease in the wave heights between 3% and 18%, for the density of 50 stems/m^2, and between 3% and 35%, for the density of 100 stems/m^2.

It was expected to get lower reduction of the wave heights comparing to the results of Sierra et al., 2017. Please note that this study does not address stem heights above 20 cm, as this is the height reached by *Zostera noltei* at the southern Romanian coast.

4.2. *Wave agitation and wave energy*

An example of calculating the Wave Agitation and Wave Energy in one point is given in the Appendix C.

The results for all the points along the three transects (Fig. 7) are reported in Tables 4 and 5 and in Figs. 14 and 15**.** The locations of the points with respect to the vegetation meadow, are also reported in the Tables 4 and 5**.**

Along the north transect, the points N2 and N3 are located between the shoreline and the vegetation meadow. The point N4 is located at the edge of the vegetation meadow. The points N5 to N9 are located within the vegetation meadow, while the point N10 is located outside of it.

Along the central transect, the points C2 and C3 are located between the shoreline and the vegetation meadow. The points C4 to C9 are located within the vegetation meadow, while the point C10 is located outside of it.

Along the south transect, the point S3 is located between the

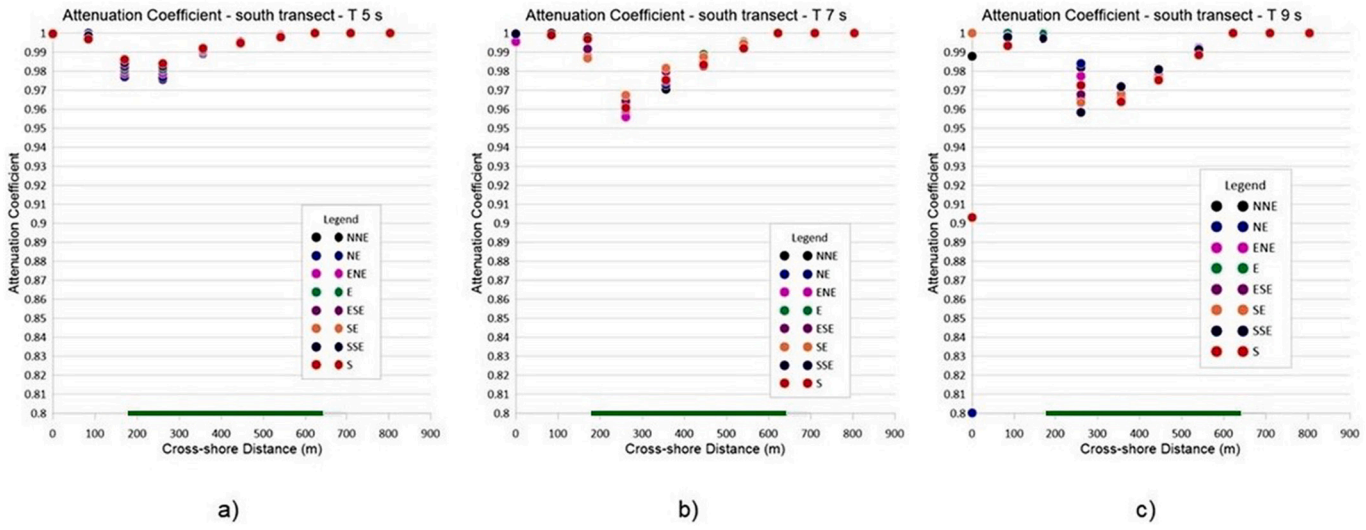

Fig. 13. Attenuation coefficient versus cross-shore distance along the south transect through the vegetation meadow for mean wave periods: a) 5 s; b) 7 s; c) 9 s. The green line on the horizontal axis marks the extent of the vegetation meadow along the transect. (For interpretation of the references to colour in this figure legend, the reader is referred to the web version of this article.) (For interpretation of the references to colour in this figure legend, the reader is referred to the web version of this article.)

Table 3
Highest attenuation on transects; the points are shown on Fig. 7.

Point	Distance (m)	Wave Direction	Mean Wave Period (s)	K_d
North transect				
N4	230.03	SSE	5	0.9485
N4	230.03	NE	7	0.9121
N5	321.01	E	9	0.9137
Central transect				
C3	157.01	NE	5	0.9529
C4	253.05	E	7	0.9316
C4	253.05	SSE	9	0.9284
South transect				
S4	260.07	NNE	5	0.9756
S4	260.07	ENE	7	0.9558
S1	0	NE	9	0.8003

shoreline and the vegetation meadow. The points S4 to S8 are located within the vegetation meadow, while the points S9 and S10 are located outside of it.

We are taking into account Wave Agitation and Wave Energy reduction values of at least 1%. Lower values of reduction should be understood as within the uncertainty band of the modelling approach. Therefore, values below 1% have not been considered as significant.

Wave Agitation reduction is over 1% in the following points (Table 4): N2 to N7 (cross-shore distance 53 to 522 m and 0.63 to 3.84 m deep); C3 to C9 (cross-shore distance 157 to 752 m and 1.56 to 4.6 m deep); S3 to S5 (cross-shore distance 170 to 356 m and 1.21 to 3.75 m deep).

Wave Energy reduction is over 1% in the following points (Table 5): N2 to N9 (cross-shore distance 53 to 714 m and 0.63 to 5.12 m deep); C2 to C10 (cross-shore distance 64 to 847 m and 0.74 to 4.87 m deep); S3 to S6 (cross-shore distance 170 to 445 m and 1.21 to 4.94 m deep).

Reduction in Wave Agitation reaches >10% in one point in the central part of the north transect, at >400 m from the shoreline and over 3 m deep, and in three points along the central transect, at >500 m from the shoreline and at depths between 4.3 and 4.6 m. Along the south transect, reduction in Wave Agitation reaches >8% at over 350 m from the shoreline and 3.75 m deep. (Fig. 7 and Table 4).

Along the north transect, reduction in Wave Energy reaches >10% between the shoreline and the vegetation meadow, as well as inside the vegetation meadow, between 230 m from the shoreline and 2 m deep, and over 400 m and 3 m deep. Waves from SSE and S, with rather significant frequencies of occurrence (Tables A.7 and A.8), travel more through the vegetation meadow before reaching the points located in the central part of the north transect, which show Wave Energy attenuation over 10%.

Along the central transect, reduction in Wave Energy reaches over 10%, inside the vegetation meadow, at >500 m from the shoreline and 4.3–4.5 m deep. Along the south transect, the maximum reduction in Wave Energy is 5%, inside the vegetation meadow, at 260 m from the shoreline and 2 m deep (Fig. 7 and Table 5).

The highest reduction values are reached in the point C7, at 551 m from the shoreline and 4.36 m deep – 17.89% for Wave Agitation and 16.60% for Wave Energy (Tables 4 and 5). As already discussed on the values of the attenuation coefficient, waves from NNE, NE, ENE, and S sectors travel more through the vegetation meadow before reaching the central transect. These waves also show higher frequencies of occurrence (Tables A.1, A.2, A.3, and A.8) comparing to the other sectors. Note that there is also the small elevated zone located east of the vegetation meadow, that is an obstacle for the offshore waves, especially coming from the eastern sectors. All these factors lead to more attenuation along the central transect.

Southern waves do not interact excessively with the vegetation meadow, prior to reach the south transect points. That may be a plausible reason for justifying whether Wave Agitation and Wave Energy show the lowest reduction along the south transect (Tables 4 and 5).

4.3. Simulations considering less extended vegetation masks

The already shown vegetated area extends about 1.5 km alongshore, with a maximum width of 650 m, between 2 and 6 m deep. In order to assess the model sensitivity, a less extended (i.e. narrower) vegetated area has also been addressed. Hence, the same 72 simulations have been run with a vegetation mask with the same alongshore extension, but with the width reduced by half comparing to the initial one, that is of about 300 m. This narrow mask is denoted as NM1. It reaches between 4 m deep in the northern and central parts and 5 m deep in the southern part.

Additionally, a second vegetated area layout has been considered, with the same alongshore extension and about 300 m wide, covering the 'offshore half' of the initial vegetation mask. This second narrow mask is denoted as NM2 and extends between 4 and 6 m deep. The same 72

Table 4
Wave Agitation (m) in transects through the vegetation meadow; the points are shown on Fig. 7.

Point	Cross-shore Distance (m)	Water Depth (m)	Scenario		Wave Agitation reduction (%)	Location with respect to the vegetation meadow
			Baseline	Vegetation		
North transect						
N1	0	0.2015	0.00699	0.00700	No reduction	shoreline - vegetation
N2	53.04	0.6345	0.01863	0.01825	**2.04**	shoreline - vegetation
N3	139.09	1.338	0.02973	0.02734	**8.04**	shoreline - vegetation
N4	230.03	2.007	0.03985	0.03650	**8.41**	edge vegetation
N5	321.01	2.575	0.04970	0.04741	**4.61**	inside
N6	415.02	3.141	0.05001	0.04432	**11.38**	inside
N7	522.02	3.844	0.05234	0.05074	**3.06**	inside
N8	612.01	4.391	0.05343	0.05295	0.90	inside
N9	714.01	5.125	0.05518	0.05490	0.51	inside
N10	804.00	5.840	0.05742	0.05739	0.05	outside
Central transect						
C1	0	0.1346	0.00541	0.00542	No reduction	shoreline - vegetation
C2	64.03	0.7394	0.02490	0.02466	0.96	shoreline - vegetation
C3	157.01	1.562	0.05286	0.05112	**3.29**	shoreline - vegetation
C4	253.05	2.354	0.06127	0.05860	**4.36**	inside
C5	342.04	3.119	0.06362	0.06226	**2.14**	inside
C6	446.05	3.974	0.06570	0.06487	**1.26**	inside
C7	551.03	4.364	0.07948	0.06526	**17.89**	inside
C8	655.05	4.483	0.07912	0.06652	**15.93**	inside
C9	752.05	4.599	0.07866	0.07007	**10.92**	inside
C10	847.07	4.867	0.07936	0.07902	0.43	outside
South transect						
S1	0	0.1313	0.0030372	0.0030356	0.05	shoreline - vegetation
S2	83.15	0.5033	0.01791	0.01789	0.11	shoreline - vegetation
S3	170.11	1.214	0.04862	0.04748	**2.34**	shoreline - vegetation
S4	260.07	2.063	0.05414	0.05280	**2.48**	inside
S5	356.04	3.754	0.05422	0.04977	**8.21**	inside
S6	445.02	4.940	0.05740	0.05685	0.96	inside
S7	541.05	5.618	0.06114	0.06092	0.36	inside
S8	622.04	6.095	0.06673	0.06673	0.00	inside
S9	710.03	6.637	0.08501	0.08501	0.00	outside
S10	804.05	7.068	0.10375	0.10375	0.00	outside

simulations have been run with this second narrow mask as well.

Both narrow masks are shown on Fig. 16.

For both narrow masks, the results of these simulations show extremely low differences in the calculated wave heights, with respect to the Baseline Scenario, in the order of mm in few points, along the northern and central transects, and only for the waves from the NE sector with the mean period of 9 s.

In these specific conditions, the highest differences in wave heights occur in the point N10–6 mm for NM1 and 10 mm for NM2. In the case of NM2, this gives a maximum reduction in wave heights, from 1.595 m to 1.585 m, which means 0.63%. In terms of wave energy, it gives a maximum reduction from 1583.20 J/m^2 to 1563.41 J/m^2, which means 1.25%.

Taking these results into account, the model shows very low sensitivity if the narrow vegetation masks NM1 (2 to 5 m deep) or NM2 (4 to 6 m deep), are added to the domain. Hence, it can be concluded that the two narrow masks are not effective in reducing wave heights and wave energy in the study area, for the present-day wave climate.

Following these attempts, we can state that specific vegetation belts are not suitable for the southern Romanian coast, due to their fairly low impact on wave height and wave energy reduction.

Only a well-developed *Zostera noltei* meadow, between 2 and 6 m deep, could have a significant impact and, thus, be considered as a nature-based solution for coastal protection. This is consistent with Bradley and Houser, 2009, who state that the ability of seagrass to attenuate wave energy is the result of its density and extent.

5. Discussion

Even if recent studies show that there is interest in the use of seagrass as a nature-based solution for coastal protection, research is mainly focused on its impact as to provide shelter and food for specific fauna. Previous research has seldom addressed the protection ecosystem service for the western Black Sea coast.

In our study we have checked a healthy mature seagrass in the area. Surugiu, 2008 states that the maximum stem height of *Zostera noltei* along the Romanian Black Sea coast is around 20 cm. We chose this stem height for our simulations, assuming that a lower value wouldn't lead to wave attenuation, while a higher one would be unrealistic. We have also considered a realistic value of the stem density of 100 stems/m^2 for our study area, as it is not sheltered.

The results of our study clearly indicate a relationship between the *Zostera noltei* meadow width and wave attenuation. Storm events that will enter in breaking conditions at depths between 2 and 6 m (coinciding with the location of the meadow) will suffer a reduction of the wave height in case of crossing the seagrass meadow. Such reduction will have an effect on the induced longshore sediment transport, that depends on the wave height at a power of 2.5, according to the CERC formula (Shore Protection Manual, 1984). Thus, a reduction of 5% of the wave height at breaking will induce a reduction of 12% of the longshore sediment transport.

There are points where the calculated attenuation coefficients are slightly over 1, for certain wave conditions. There are also points where the attenuation coefficients are slightly smaller than 1. In such points, attenuation can be considered negligible.

The points where the attenuation coefficients can be slightly over 1

Table 5
Wave Energy density (J/m^2) in transects through the vegetation meadow; the points are shown on Fig. 7.

Point	Cross-shore Distance (m)	Water Depth (m)	Scenario		Wave Energy reduction (%)	Location with respect to the vegetation meadow
			Baseline	Vegetation		
North transect						
N1	0	0.2015	0.3714	0.3728	No reduction	shoreline - vegetation
N2	53.04	0.6345	2.6721	2.5713	**3.77**	shoreline - vegetation
N3	139.09	1.338	6.6742	5.8435	**12.45**	shoreline - vegetation
N4	230.03	2.007	11.3153	9.7966	**13.42**	edge vegetation
N5	321.01	2.575	15.9950	14.4445	**9.69**	inside
N6	415.02	3.141	16.2837	13.8775	**14.78**	inside
N7	522.02	3.844	17.8852	16.8399	**5.84**	inside
N8	612.01	4.391	18.7214	18.2657	**2.43**	inside
N9	714.01	5.125	19.8007	19.5522	**1.26**	inside
N10	804.00	5.840	21.2167	21.1922	0.12	outside
Central transect						
C1	0	0.1346	0.2527	0.2534	No reduction	shoreline - vegetation
C2	64.03	0.7394	4.7175	4.6298	**1.86**	shoreline - vegetation
C3	157.01	1.562	16.5128	15.5471	**5.85**	shoreline - vegetation
C4	253.05	2.354	23.7369	21.7067	**8.55**	inside
C5	342.04	3.119	26.5962	25.0361	**5.87**	inside
C6	446.05	3.974	28.4252	27.2149	**4.26**	inside
C7	551.03	4.364	33.4826	27.9236	**16.60**	inside
C8	655.05	4.483	33.2253	28.8352	**13.21**	inside
C9	752.05	4.599	32.4845	29.2497	**9.96**	inside
C10	847.07	4.867	32.8254	32.4809	**1.05**	outside
South transect						
S1	0	0.1313	0.0705	0.0703	0.28	shoreline - vegetation
S2	83.15	0.5033	2.4410	2.4365	0.18	shoreline - vegetation
S3	170.11	1.214	13.6774	13.1918	**3.55**	shoreline - vegetation
S4	260.07	2.063	20.0485	19.0340	**5.06**	inside
S5	356.04	3.754	18.9582	18.2077	**3.96**	inside
S6	445.02	4.940	21.0776	20.5853	**2.34**	inside
S7	541.05	5.618	23.9967	23.7807	0.90	inside
S8	622.04	6.095	27.2390	27.2389	0.00	inside
S9	710.03	6.637	35.2607	35.2607	0.00	outside
S10	804.05	7.068	44.0529	44.0529	0.00	outside

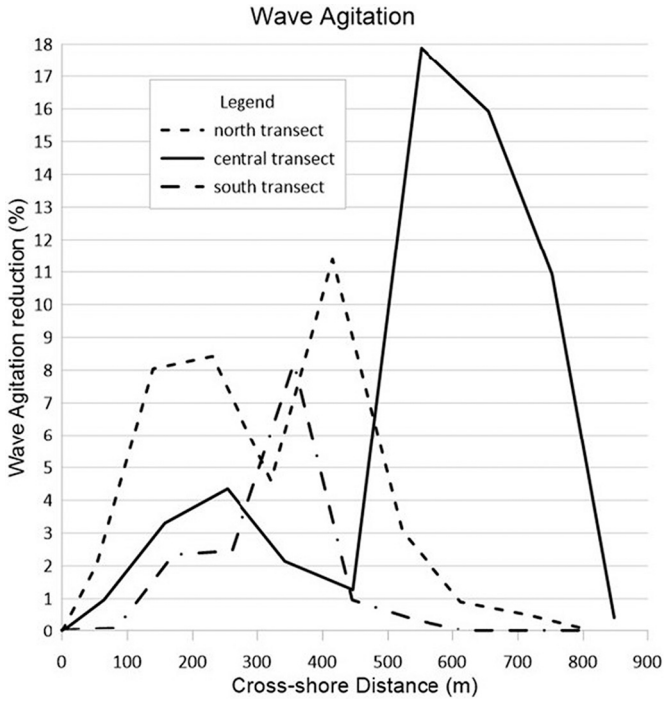

Fig. 14. Wave Agitation along the north (dashed line), central (solid line) and south (dash-dotted) transects.

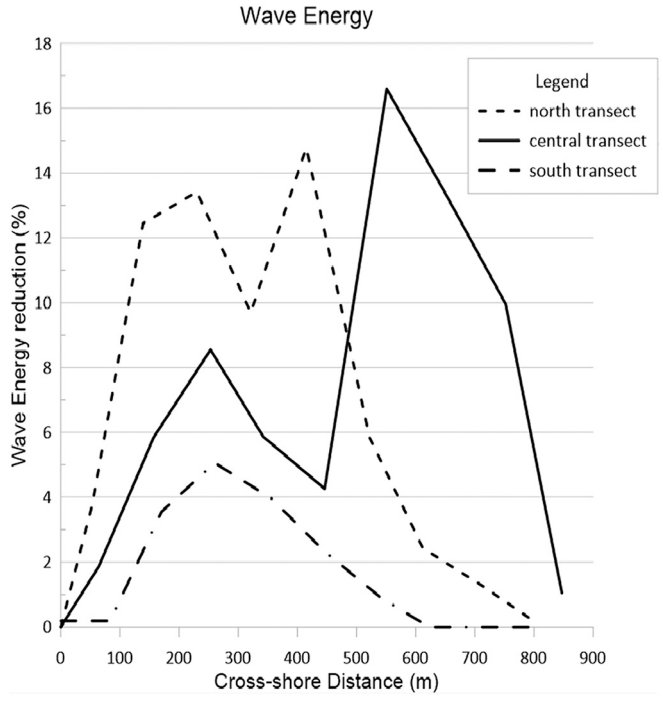

Fig. 15. Wave Energy density along the north (dashed line), central (solid line) and south (dash-dotted line) transects.

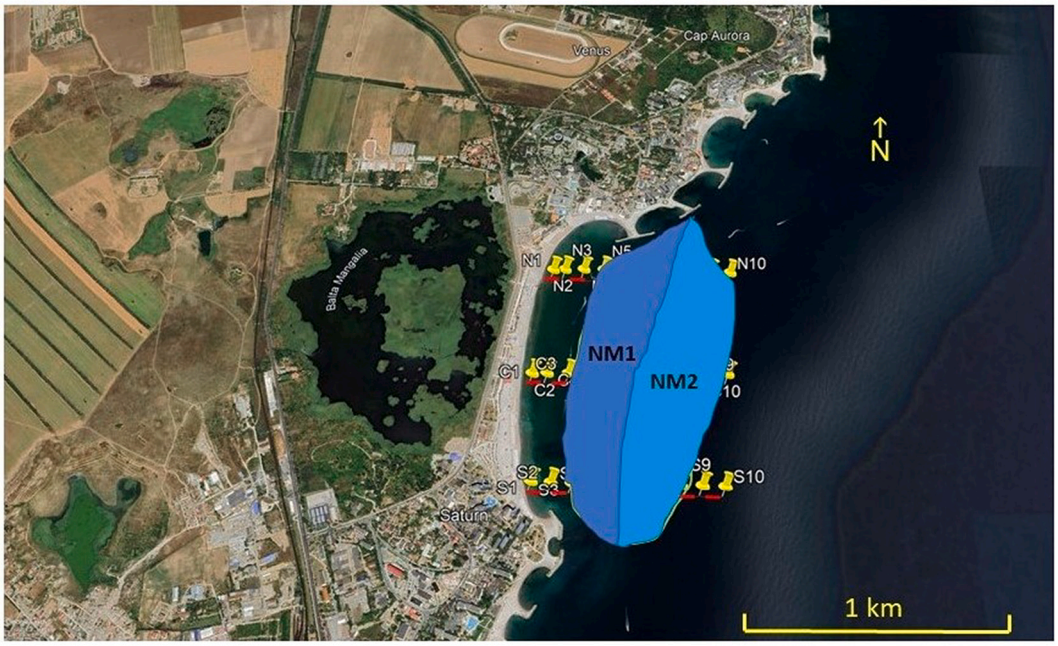

Fig. 16. The two narrow masks, NM1 and NM2, used in the analysis.

are located between the shoreline and the vegetation meadow. These are: N1, N2, C1, C2, S1, S2. All these points have depths <1 m. Moreover, similar small differences may occur in the points N3, C3, S3, with depths between 1.2 and 1.6 m, but only for certain wave conditions.

It becomes obvious that there are points where the calculated wave height attenuation is of the same order of magnitude than the so-called 'amplification' of the wave heights, mentioned above. Thus, we appreciate that wave height differences between the Baseline and Vegetation scenarios that are lower than 1 cm should be disregarded, even if they may suggest a light attenuation.

The effect of the vegetation meadow within a typical year has been estimated by summing up the effects of all the considered storms, with their specific frequencies of occurrence. The most significant reduction in Wave Agitation is almost 18%. The most significant reduction in Wave Energy is 16.6%. Both reduction values occur on the central transect and are influenced by the extent of the vegetation meadow, the wave climate, and the local bathymetry.

We cannot consider this green solution as very effective in the initial stages or for limited size meadows. From a wave dynamics point of view, seagrass is less efficient in the short term than grey solutions. This is due especially to the limitations related to the characteristics of the *Zostera noltei* species, that cannot exceed certain values of stem height and stem density at the latitudes of the study area.

Even if the wave height reduction by the vegetation meadow is not spectacular, the reduction in Wave Agitation and Wave Energy suggests that this green measure could be regarded as an additional solution for coastal protection, where appropriate. A combination of grey and green solutions may prove to be effective across time scales and climate scenarios, in many parts of a coast. But our specific study area is in front of a protected Natura 2000 site, therefore grey solutions are not recommended.

Zostera noltei meadows do not have immediate effect in reducing the wave height and energy, as they must reach wide dimensions, so it takes time for them to develop. But this species can develop naturally along the southern Romanian coast. Once developed, it can provide benefits to the ecosystem, as it may enhance biodiversity (Surugiu et al., 2021). Because of this, as in many other Nature based Solutions, *Zostera noltei* meadows should be included in mid- to long-term plans, as an additional protection measure to reduce wave height and energy along the southern Romanian coast. As discussed by Koch et al., 2009; Nordlund et al., 2017, although seagrass may play an important role in protecting the coast against the effect of waves and currents, it cannot be assumed that its pure presence will lead to the full provision of this ecosystem service. This is even more obvious for *Zostera noltei* along the Romanian coast, that is limited in what concerns stem height and density.

The results shown in this contribution present a moderate impact of wave damping due to *Zostera noltei* meadows on the southern Romanian coast. Nevertheless, there are significant uncertainties regarding the wave-vegetation interaction that would require further research. Improvements on the modelling accuracy can be achieved through physical modelling, using wave flume experiments (Ganthy et al., 2013b, 2015; Kombiadou et al., 2014). This could open new research topics and foster future collaborations.

The wave-climate projections used in this study were produced by Lin-Ye et al., 2018 for the northwestern part of the Black Sea. As the new ERA5 dataset is now available, it can be observed that our study could be extended in the future by using more accurate forcing, at least for present climate conditions.

Moreover, recent studies at the global level indicate that climate change may lead to increasing sea level rise (Cazenave and Le Cozannet, 2013; Church et al., 2013; Jevrejeva et al., 2014; Yi et al., 2015; Sánchez-Arcilla et al., 2016; Chen et al., 2017; Nerem et al., 2018), as well as to an increasing frequency of storm events (Hemer et al., 2013). All these may lead to increased risk for coasts (Tătui et al., 2019; Avşar and Kutoğlu, 2020). Some authors state that sea level rise may affect the development of seagrass because it leads to increased water depth and, thus, to reduced availability of light (Saunders et al., 2013; Scalpone et al., 2020). But, as discussed by Waycott et al., 2007, in the case of sea level rise, seagrass could migrate up slope and colonize newly inundated lands. Taking this into account, the perspective of sea level rise may reinforce the idea to explore the possibility to use seagrass as a soft nature-based solution for coastal protection.

Our study is a first step in the quantification of the effect of *Zostera noltei* seagrass as a Nature based Solution on the Romanian coast. As suggested by Nordlund et al., 2017, a comprehensive assessment of ecosystem services is still lacking for *Zostera* species of seagrass. Considering all these aspects, we appreciate that our study could be followed by a more detailed study, using updated forcing and physical

modelling.

As it has been seen, the effect of a seagrass meadow depends on the combination of biological and physical factors. The first ones consider aspects such as the stem height and density, as well as the meadow geometry, whereas the second refers to the hydrodynamic conditions impacting on the coast, such as the wave height, period and direction and its occurrence within a typical year. The results obtained in this study can be extrapolated to coastal stretches with similar conditions, i.e. fetch limited environments and enclosed beaches of about 1.5 km. Moreover, the proposed methodology can be applied to other sandy beaches where seagrass can have appropriate conditions to develop.

6. Conclusions

This work aims to provide a quantitative assessment of a *Zostera noltei* meadow effect on coastal protection for an area located on the southern Romanian coast, between the Venus and Saturn resorts, given the recent interest in specific seagrass regeneration projects.

Various numerical simulations have been performed, using a calibrated SWAN model, for present-day wave forcings, first in the absence of the vegetation meadow, then adding it to the setup. We have simulated the presence of a well-developed *Zostera noltei* meadow, extended from 2 to 6 m depth and with the maximum stem height that it may reach.

The results have been analysed along three transects through the *Zostera noltei* meadow. Waves from the northeastern and south sectors, that have high frequencies of occurrence, travel longer across the vegetation meadow, due to its shape, thus being subject to the most significant attenuation.

Our study suggests that only a well-developed vegetation meadow could have an impact on wave height and energy in the study area, indicating that development time should also be considered in the assessments.

This work, based on numerical modelling for various wave forcings, may provide a good experience in what concerns the analysis of the impact of green measures. This type of approach, based on wave projections for the present climate, could be useful in discussing possible coastal protection solutions with local stakeholders. Besides, the proposed methodology could also be applied in other parts of the world, with sandy beaches, where seagrass might have appropriate conditions to develop.

Author contributions

Irina Dinu performed the SWAN simulations, analysed the model outputs and led the paper. Albert Monclús i Bori performed the preliminary wave climate analysis, together with Manuel García-León and Jue Lin-Ye, that served as basis for the work of Irina Dinu. Vicente Gràcia supervised the work and provided expertise on Oceanography and Nature based solutions. Adrian Stănică and Agustín Sánchez-Arcilla provided expertise on Oceanography and contributed in the analysis of results. Several proof-readings have been held by all co-authors via videoconference meetings.

Declaration of Competing Interest

The authors declare that they have no known competing financial interests or personal relationships that could have appeared to influence the work reported in this paper. The funding sources had no role in the design of the study, in the analysis and interpretation of data; in the writing of the manuscript, and in the decision to publish the results.

Data availability

Data will be made available on request.

Acknowledgements

The idea of this work came up following the FP7 RISES-AM project, GA 603396, funded by the FP7-ENV-2013-two stage program of the European Commission. The first author acknowledges the mobility projects MC2017-1274 and MC2018-1922, funded by the Romanian Authority for Scientific Research, covering the expenses of two research visits at the Maritime Engineering Laboratory of the Polytechnic University of Catalonia Barcelona Tech (LIM-UPC), during which work on this topic started. This work was partially supported by the Spanish Government within the Research, Development and Innovation Program through the grant to ECOPLANTS project (Ref. PID2020-119058RB-I00). The REST-COAST Horizon 2020 Research and Innovation Grant 101037097 has also contributed to finance some of the authors. The rest of the work has been performed within the projects PN 18160103 and PN 19200201, funded by the Ministry of Research, Innovation and Digitization of Romania and H2020 DOORS (EC Grant Agreement 101000518). We acknowledge as well the valuable comments of an anonymous reviewer, which allowed us to significantly improve the manuscript.

Appendix A. Tables of occurrence

The following tables show the frequencies of occurrence, computed for each wave direction, as discussed at the '3.1. Input data' subsection from the '3. Methodology' section.

Table A.1
Frequencies of occurrence for the NNE wave direction.

		T_p (s)							
		0–2	2–4	4–6	6–8	8–10	10–12	> 12	**Total**
H_s (m)	0–0.5	0.00030	0.02640	0.00640	0.00034	0.00044	0.00000	0.00000	**0.03388**
	0.5–1	0.00000	0.02691	0.01594	0.00146	0.00061	0.00000	0.00000	**0.04492**
	1–1.5	0.00000	0.00068	0.02850	0.00125	0.00010	0.00000	0.00000	**0.03053**
	1.5–2	0.00000	0.00000	0.01784	0.00146	0.00024	0.00000	0.00000	**0.01953**
	2–2.5	0.00000	0.00000	0.00545	0.00427	0.00017	0.00000	0.00000	**0.00988**
	2.5–3	0.00000	0.00000	0.00020	0.00663	0.00017	0.00000	0.00000	**0.00701**
	3–3.5	0.00000	0.00000	0.00000	0.00440	0.00003	0.00000	0.00000	**0.00443**
	3.5–4	0.00000	0.00000	0.00000	0.00271	0.00027	0.00000	0.00000	**0.00298**
	4–4.5	0.00000	0.00000	0.00000	0.00058	0.00081	0.00000	0.00000	**0.00139**

(*continued on next page*)

Table A.1 (*continued*)

		T_p (s)							
		0–2	2–4	4–6	6–8	8–10	10–12	> 12	**Total**
	4.5–5	0.00000	0.00000	0.00000	0.00010	0.00051	0.00000	0.00000	**0.00061**
	5–5.5	0.00000	0.00000	0.00000	0.00000	0.00017	0.00000	0.00000	**0.00017**
	5.5–6	0.00000	0.00000	0.00000	0.00000	0.00017	0.00000	0.00000	**0.00017**
	6–6.5	0.00000	0.00000	0.00000	0.00000	0.00003	0.00000	0.00000	**0.00003**
	6.5–7	0.00000	0.00000	0.00000	0.00000	0.00000	0.00000	0.00000	**0.00000**
	7–7.5	0.00000	0.00000	0.00000	0.00000	0.00000	0.00000	0.00000	**0.00000**
	7.5–8	0.00000	0.00000	0.00000	0.00000	0.00000	0.00000	0.00000	**0.00000**
	8–8.5	0.00000	0.00000	0.00000	0.00000	0.00000	0.00000	0.00000	**0.00000**
	8.5–9	0.00000	0.00000	0.00000	0.00000	0.00000	0.00000	0.00000	**0.00000**
	9–9.5	0.00000	0.00000	0.00000	0.00000	0.00000	0.00000	0.00000	**0.00000**
	9.5–10	0.00000	0.00000	0.00000	0.00000	0.00000	0.00000	0.00000	**0.00000**
	> 10	0.00000	0.00000	0.00000	0.00000	0.00000	0.00000	0.00000	**0.00000**
Total		**0.00030**	**0.05399**	**0.07433**	**0.02319**	**0.00372**	**0.00000**	**0.00000**	**0.15554**

Table A.2
Frequencies of occurrence for the NE wave direction.

		T_p (s)							
		0–2	2–4	4–6	6–8	8–10	10–12	> 12	**Total**
H_s (m)	0–0.5	0.00037	0.03751	0.01601	0.00041	0.00034	0.00000	0.00000	**0.05463**
	0.5–1	0.00000	0.02914	0.03162	0.00196	0.00081	0.00000	0.00000	**0.06354**
	1–1.5	0.00000	0.00058	0.03067	0.00406	0.00030	0.00000	0.00000	**0.03561**
	1.5–2	0.00000	0.00000	0.01642	0.00592	0.00007	0.00000	0.00000	**0.02241**
	2–2.5	0.00000	0.00000	0.00332	0.01100	0.00014	0.00000	0.00000	**0.01445**
	2.5–3	0.00000	0.00000	0.00017	0.00714	0.00017	0.00000	0.00000	**0.00748**
	3–3.5	0.00000	0.00000	0.00000	0.00345	0.00112	0.00000	0.00000	**0.00457**
	3.5–4	0.00000	0.00000	0.00000	0.00112	0.00156	0.00000	0.00000	**0.00267**
	4–4.5	0.00000	0.00000	0.00000	0.00014	0.00098	0.00000	0.00000	**0.00112**
	4.5–5	0.00000	0.00000	0.00000	0.00000	0.00071	0.00000	0.00000	**0.00071**
	5–5.5	0.00000	0.00000	0.00000	0.00000	0.00030	0.00000	0.00000	**0.00030**
	5.5–6	0.00000	0.00000	0.00000	0.00000	0.00010	0.00000	0.00000	**0.00010**
	6–6.5	0.00000	0.00000	0.00000	0.00000	0.00000	0.00000	0.00000	**0.00000**
	6.5–7	0.00000	0.00000	0.00000	0.00000	0.00000	0.00000	0.00000	**0.00000**
	7–7.5	0.00000	0.00000	0.00000	0.00000	0.00000	0.00000	0.00000	**0.00000**
	7.5–8	0.00000	0.00000	0.00000	0.00000	0.00000	0.00000	0.00000	**0.00000**
	8–8.5	0.00000	0.00000	0.00000	0.00000	0.00000	0.00000	0.00000	**0.00000**
	8.5–9	0.00000	0.00000	0.00000	0.00000	0.00000	0.00000	0.00000	**0.00000**
	9–9.5	0.00000	0.00000	0.00000	0.00000	0.00000	0.00000	0.00000	**0.00000**
	9.5–10	0.00000	0.00000	0.00000	0.00000	0.00000	0.00000	0.00000	**0.00000**
	> 10	0.00000	0.00000	0.00000	0.00000	0.00000	0.0000	0.0000	**0.00000**
Total		**0.00037**	**0.06723**	**0.09820**	**0.03520**	**0.00660**	**0.0000**	**0.0000**	**0.20760**

Table A.3
Frequencies of occurrence for the ENE wave direction.

		T_p (s)							
		0–2	2–4	4–6	6–8	8–10	10–12	> 12	**Total**
H_s (m)	0–0.5	0.00068	0.03151	0.01459	0.00152	0.00020	0.00000	0.00000	**0.04851**
	0.5–1	0.00000	0.01689	0.02271	0.00443	0.00196	0.00000	0.00000	**0.04600**
	1–1.5	0.00000	0.00041	0.01577	0.00332	0.00105	0.00000	0.00000	**0.02055**
	1.5–2	0.00000	0.00000	0.00582	0.00433	0.00027	0.00000	0.00000	**0.01043**
	2–2.5	0.00000	0.00000	0.00118	0.00399	0.00088	0.00000	0.00000	**0.00606**
	2.5–3	0.00000	0.00000	0.00000	0.00284	0.00095	0.00000	0.00000	**0.00379**
	3–3.5	0.00000	0.00000	0.00000	0.00112	0.00098	0.00000	0.00000	**0.00210**
	3.5–4	0.00000	0.00000	0.00000	0.00037	0.00166	0.00000	0.00000	**0.00203**
	4–4.5	0.00000	0.00000	0.00000	0.00010	0.00105	0.00000	0.00000	**0.00115**
	4.5–5	0.00000	0.00000	0.00000	0.00000	0.00061	0.00000	0.00000	**0.00061**
	5–5.5	0.00000	0.00000	0.00000	0.00000	0.00014	0.00000	0.00000	**0.00014**
	5.5–6	0.00000	0.00000	0.00000	0.00000	0.00003	0.00000	0.00000	**0.00003**
	6–6.5	0.00000	0.00000	0.00000	0.00000	0.00000	0.00000	0.00000	**0.00000**
	6.5–7	0.00000	0.00000	0.00000	0.00000	0.00000	0.00000	0.00000	**0.00000**
	7–7.5	0.00000	0.00000	0.00000	0.00000	0.00000	0.00000	0.00000	**0.00000**
	7.5–8	0.00000	0.00000	0.00000	0.00000	0.00000	0.00000	0.00000	**0.00000**
	8–8.5	0.00000	0.00000	0.00000	0.00000	0.00000	0.00000	0.00000	**0.00000**
	8.5–9	0.00000	0.00000	0.00000	0.00000	0.00000	0.00000	0.00000	**0.00000**
	9–9.5	0.00000	0.00000	0.00000	0.00000	0.00000	0.00000	0.00000	**0.00000**

(*continued on next page*)

Table A.3 (*continued*)

		T_p (s)							
		0–2	2–4	4–6	6–8	8–10	10–12	> 12	**Total**
	9.5–10	0.00000	0.00000	0.00000	0.00000	0.00000	0.00000	0.00000	**0.00000**
	> 10	0.00000	0.00000	0.00000	0.00000	0.00000	0.00000	0.00000	**0.00000**
Total		**0.00068**	**0.04881**	**0.06008**	**0.02204**	**0.00978**	**0.00000**	**0.00000**	**0.14139**

Table A.4
Frequencies of occurrence for the E wave direction.

		T_p (s)							
		0–2	2–4	4–6	6–8	8–10	10–12	> 12	**Total**
H_s (m)	0–0.5	0.00044	0.01737	0.01080	0.00179	0.00037	0.00000	0.000000	**0.03077**
	0.5–1	0.00000	0.01066	0.01713	0.01029	0.00237	0.00000	0.00000	**0.04045**
	1–1.5	0.00000	0.00007	0.00677	0.00660	0.00176	0.00000	0.00000	**0.01520**
	1.5–2	0.00000	0.00000	0.00301	0.00349	0.00152	0.00000	0.00000	**0.00802**
	2–2.5	0.00000	0.00000	0.00037	0.00210	0.00085	0.00000	0.00000	**0.00332**
	2.5–3	0.00000	0.00000	0.00000	0.00105	0.00091	0.00000	0.00000	**0.00196**
	3–3.5	0.00000	0.00000	0.00000	0.00027	0.00054	0.00000	0.00000	**0.00081**
	3.5–4	0.00000	0.00000	0.00000	0.00000	0.00085	0.00000	0.00000	**0.00085**
	4–4.5	0.00000	0.00000	0.00000	0.00000	0.00020	0.00000	0.00000	**0.00020**
	4.5–5	0.00000	0.00000	0.00000	0.00000	0.00014	0.00000	0.00000	**0.00014**
	5–5.5	0.00000	0.00000	0.00000	0.00000	0.00010	0.00000	0.00000	**0.00010**
	5.5–6	0.00000	0.00000	0.00000	0.00000	0.00003	0.00000	0.00000	**0.00003**
	6–6.5	0.00000	0.00000	0.00000	0.00000	0.00000	0.00000	0.00000	**0.00000**
	6.5–7	0.00000	0.00000	0.00000	0.00000	0.00000	0.00000	0.00000	**0.00000**
	7–7.5	0.00000	0.00000	0.00000	0.00000	0.00000	0.00000	0.00000	**0.00000**
	7.5–8	0.00000	0.00000	0.00000	0.00000	0.00000	0.00000	0.00000	**0.00000**
	8–8.5	0.00000	0.00000	0.00000	0.00000	0.00000	0.00000	0.00000	**0.00000**
	8.5–9	0.00000	0.00000	0.00000	0.00000	0.00000	0.00000	0.00000	**0.00000**
	9–9.5	0.00000	0.00000	0.00000	0.00000	0.00000	0.00000	0.00000	**0.00000**
	9.5–10	0.00000	0.00000	0.00000	0.00000	0.00000	0.00000	0.00000	**0.00000**
	> 10	0.00000	0.00000	0.00000	0.00000	0.00000	0.00000	0.00000	**0.00000**
Total		**0.00044**	**0.02810**	**0.03808**	**0.02559**	**0.00965**	**0.00000**	**0.00000**	**0.10185**

Table A.5
Frequencies of occurrence for the ESE wave direction.

		T_p (s)							
		0–2	2–4	4–6	6–8	8–10	10–12	> 12	**Total**
H_s (m)	0–0.5	0.00061	0.01865	0.00985	0.00098	0.00034	0.00000	0.00000	**0.03043**
	0.5–1	0.00000	0.00883	0.01493	0.00667	0.00088	0.00000	0.00000	**0.03131**
	1–1.5	0.00000	0.00017	0.00657	0.00562	0.00115	0.00000	0.00000	**0.01351**
	1.5–2	0.00000	0.00000	0.00169	0.00308	0.00078	0.00000	0.00000	**0.00555**
	2–2.5	0.00000	0.00000	0.00020	0.00159	0.00078	0.00000	0.00000	**0.00257**
	2.5–3	0.00000	0.00000	0.00003	0.00078	0.00061	0.00000	0.00000	**0.00142**
	3–3.5	0.00000	0.00000	0.00000	0.00007	0.00030	0.00000	0.00000	**0.00037**
	3.5–4	0.00000	0.00000	0.00000	0.00003	0.00037	0.00000	0.00000	**0.00041**
	4–4.5	0.00000	0.00000	0.00000	0.00000	0.00010	0.00000	0.00000	**0.00010**
	4.5–5	0.00000	0.00000	0.00000	0.00000	0.00003	0.00000	0.00000	**0.00003**
	5–5.5	0.00000	0.00000	0.00000	0.00000	0.00000	0.00000	0.00000	**0.00000**
	5.5–6	0.00000	0.00000	0.00000	0.00000	0.00000	0.00000	0.00000	**0.00000**
	6–6.5	0.00000	0.00000	0.00000	0.00000	0.00000	0.00000	0.00000	**0.00000**
	6.5–7	0.00000	0.00000	0.00000	0.00000	0.00000	0.00000	0.00000	**0.00000**
	7–7.5	0.00000	0.00000	0.00000	0.00000	0.00000	0.00000	0.00000	**0.00000**
	7.5–8	0.00000	0.00000	0.00000	0.00000	0.00000	0.00000	0.00000	**0.00000**
	8–8.5	0.00000	0.00000	0.00000	0.00000	0.00000	0.00000	0.00000	**0.00000**
	8.5–9	0.00000	0.00000	0.00000	0.00000	0.00000	0.00000	0.00000	**0.00000**
	9–9.5	0.00000	0.00000	0.00000	0.00000	0.00000	0.00000	0.00000	**0.00000**
	9.5–10	0.00000	0.00000	0.00000	0.00000	0.00000	0.00000	0.00000	**0.00000**
	> 10	0.00000	0.00000	0.00000	0.00000	0.00000	0.0000	0.00000	**0.00000**
Total		**0.00061**	**0.02766**	**0.03327**	**0.01882**	**0.00535**	**0.00000**	**0.00000**	**0.08571**

Table A.6
Frequencies of occurrence for the SE wave direction.

		T_p (s)							
		0–2	2–4	4–6	6–8	8–10	10–12	> 12	**Total**
H_s (m)	0–0.5	0.00068	0.02231	0.00508	0.00139	0.00030	0.00000	0.00000	**0.02975**
	0.5–1	0.00000	0.01117	0.00836	0.00234	0.00074	0.00000	0.00000	**0.02261**
	1–1.5	0.00000	0.00037	0.00464	0.00132	0.00044	0.00000	0.00000	**0.00677**
	1.5–2	0.00000	0.00000	0.00190	0.00058	0.00010	0.00000	0.00000	**0.00257**
	2–2.5	0.00000	0.00000	0.00034	0.00034	0.00037	0.00000	0.00000	**0.00105**
	2.5–3	0.00000	0.00000	0.00007	0.00024	0.00020	0.00000	0.00000	**0.00051**
	3–3.5	0.00000	0.00000	0.00000	0.00007	0.00007	0.00000	0.00000	**0.00014**
	3.5–4	0.00000	0.00000	0.00000	0.00003	0.00003	0.00000	0.00000	**0.00007**
	4–4.5	0.00000	0.00000	0.00000	0.00003	0.00003	0.00000	0.00000	**0.00007**
	4.5–5	0.00000	0.00000	0.00000	0.00000	0.00000	0.00000	0.00000	**0.00000**
	5–5.5	0.00000	0.00000	0.00000	0.00000	0.00007	0.00000	0.00000	**0.00007**
	5.5–6	0.00000	0.00000	0.00000	0.00000	0.00000	0.00000	0.00000	**0.00000**
	6–6.5	0.00000	0.00000	0.00000	0.00000	0.00000	0.00000	0.00000	**0.00000**
	6.5–7	0.00000	0.00000	0.00000	0.00000	0.00000	0.00000	0.00000	**0.00000**
	7–7.5	0.00000	0.00000	0.00000	0.00000	0.00000	0.00000	0.00000	**0.00000**
	7.5–8	0.00000	0.00000	0.00000	0.00000	0.00000	0.00000	0.00000	**0.00000**
	8–8.5	0.00000	0.00000	0.00000	0.00000	0.00000	0.00000	0.00000	**0.00000**
	8.5–9	0.00000	0.00000	0.00000	0.00000	0.00000	0.00000	0.00000	**0.00000**
	9–9.5	0.00000	0.00000	0.00000	0.00000	0.00000	0.00000	0.00000	**0.00000**
	9.5–10	0.00000	0.00000	0.00000	0.00000	0.00000	0.00000	0.00000	**0.00000**
	>10	0.00000	0.00000	0.00000	0.00000	0.00000	0.00000	0.00000	**0.00000**
Total		**0.00068**	**0.03385**	**0.02038**	**0.00633**	**0.00237**	**0.00000**	**0.00000**	**0.06360**

Table A.7
Frequencies of occurrence for the SSE wave direction.

		T_p (s)							
		0–2	2–4	4–6	6–8	8–10	10–12	> 12	**Total**
H_s (m)	0–0.5	0.00078	0.02583	0.00362	0.00037	0.00017	0.00000	0.00000	**0.03077**
	0.5–1	0.00000	0.01845	0.00836	0.00135	0.00074	0.00000	0.00000	**0.02891**
	1–1.5	0.00000	0.00051	0.00735	0.00105	0.00020	0.00000	0.00000	**0.00911**
	1.5–2	0.00000	0.00000	0.00278	0.00054	0.00024	0.00000	0.00000	**0.00355**
	2–2.5	0.00000	0.00000	0.00091	0.00061	0.00010	0.00000	0.00000	**0.00162**
	2.5–3	0.00000	0.00000	0.00007	0.00071	0.00007	0.00000	0.00000	**0.00085**
	3–3.5	0.00000	0.00000	0.00000	0.00034	0.00003	0.00000	0.00000	**0.00037**
	3.5–4	0.00000	0.00000	0.00000	0.00010	0.00000	0.00000	0.00000	**0.00010**
	4–4.5	0.00000	0.00000	0.00000	0.00007	0.00010	0.00000	0.00000	**0.00017**
	4.5–5	0.00000	0.00000	0.00000	0.00000	0.00000	0.00000	0.00000	**0.00000**
	5–5.5	0.00000	0.00000	0.00000	0.00000	0.00000	0.00000	0.00000	**0.00000**
	5.5–6	0.00000	0.00000	0.00000	0.00000	0.00000	0.00000	0.00000	**0.00000**
	6–6.5	0.00000	0.00000	0.00000	0.00000	0.00000	0.00000	0.00000	**0.00000**
	6.5–7	0.00000	0.00000	0.00000	0.00000	0.00000	0.00000	0.00000	**0.00000**
	7–7.5	0.00000	0.00000	0.00000	0.00000	0.00000	0.00000	0.00000	**0.00000**
	7.5–8	0.00000	0.00000	0.00000	0.00000	0.00000	0.00000	0.00000	**0.00000**
	8–8.5	0.00000	0.00000	0.00000	0.00000	0.00000	0.00000	0.00000	**0.00000**
	8.5–9	0.00000	0.00000	0.00000	0.00000	0.00000	0.00000	0.00000	**0.00000**
	9–9.5	0.00000	0.00000	0.00000	0.00000	0.00000	0.00000	0.00000	**0.00000**
	9.5–10	0.00000	0.00000	0.00000	0.00000	0.00000	0.00000	0.00000	**0.00000**
	> 10	0.00000	0.00000	0.00000	0.00000	0.00000	0.00000	0.00000	**0.00000**
Total		**0.00078**	**0.04478**	**0.02309**	**0.00515**	**0.00166**	**0.00000**	**0.0000**	**0.07545**

Table A.8
Frequencies of occurrence for the S wave direction.

		T_p (s)							
		0–2	2–4	4–6	6–8	8–10	10–12	> 12	**Total**
H_s (m)	0–0.5	0.00125	0.03449	0.00572	0.00068	0.00020	0.00000	0.00000	**0.04235**
	0.5–1	0.00000	0.03686	0.01933	0.00213	0.00054	0.00000	0.00000	**0.05887**
	1–1.5	0.00000	0.00081	0.02522	0.00396	0.00034	0.00000	0.00000	**0.03033**
	1.5–2	0.00000	0.00000	0.01242	0.00399	0.00047	0.00000	0.00000	**0.01689**
	2–2.5	0.00000	0.00000	0.00376	0.00667	0.00054	0.00000	0.00000	**0.01097**
	2.5–3	0.00000	0.00000	0.00003	0.00460	0.00047	0.00000	0.00000	**0.00511**
	3–3.5	0.00000	0.00000	0.00000	0.00247	0.00041	0.00000	0.00000	**0.00288**
	3.5–4	0.00000	0.00000	0.00000	0.00047	0.00041	0.00000	0.00000	**0.00088**
	4–4.5	0.00000	0.00000	0.00000	0.00007	0.00034	0.00000	0.00000	**0.00041**

(*continued on next page*)

Table A.8 (*continued*)

		T_p (s)							
		0–2	2–4	4–6	6–8	8–10	10–12	> 12	**Total**
	4.5–5	0.00000	0.00000	0.00000	0.00000	0.00007	0.00000	0.00000	**0.00007**
	5–5.5	0.00000	0.00000	0.00000	0.00000	0.00003	0.00000	0.00000	**0.00003**
	5.5–6	0.00000	0.00000	0.00000	0.00000	0.00007	0.00000	0.00000	**0.00007**
	6–6.5	0.00000	0.00000	0.00000	0.00000	0.00000	0.00000	0.00000	0.00000
	6.5–7	0.00000	0.00000	0.00000	0.00000	0.00000	0.00000	0.00000	0.00000
	7–7.5	0.00000	0.00000	0.00000	0.00000	0.00000	0.00000	0.00000	0.00000
	7.5–8	0.00000	0.00000	0.00000	0.00000	0.00000	0.00000	0.00000	0.00000
	8–8.5	0.00000	0.00000	0.00000	0.00000	0.00000	0.00000	0.00000	0.00000
	8.5–9	0.00000	0.00000	0.00000	0.00000	0.00000	0.00000	0.00000	0.00000
	9–9.5	0.00000	0.00000	0.00000	0.00000	0.00000	0.00000	0.00000	0.00000
	9.5–10	0.00000	0.00000	0.00000	0.00000	0.00000	0.00000	0.00000	0.00000
	> 10	0.00000	0.00000	0.00000	0.00000	0.00000	0.00000	0.0000	0.00000
Total		**0.00125**	**0.07217**	**0.06648**	**0.02505**	**0.00389**	**0.0000**	**0.0000**	**0.16884**

Appendix B. Results in the output points along three transects through the vegetation meadow

The following tables present the values of the calculated attenuation coefficient K_d, in all the points along the three transects shown on Fig. 7, as discussed in the subsection 3.5 from the '3. Methodology' section.

Table B.1
Results in the output points along the north transect; 'NO' means no attenuation for those specific wave conditions; the points are shown on Fig. 7.

Point / Depth (m)	H_{morf} (m)	T (s)	H_B (m)	H_V (m)	K_d
N1 / 0.2015					
NNE	1.36	5	0.08592	0.08611	1
	2.76	7	0.09195	0.09134	0.9934
	3.49	9	0.09943	0.09928	0.9985
NE	1.17	5	0.08601	0.08622	1
	2.32	7	0.09222	0.09216	0.9993
	3.53	9	0.09817	0.09919	NO
ENE	1.02	5	0.08467	0.08468	1
	1.92	7	0.09168	0.09172	1
	2.97	9	0.09974	0.09984	1
E	0.92	5	0.08382	0.08407	1
	1.37	7	0.09108	0.09127	1
	2.24	9	0.09911	0.09913	1
ESE	0.88	5	0.08314	0.08330	1
	1.40	7	0.09097	0.09106	1
	2.13	9	0.09838	0.09872	1
SE	1.00	5	0.08227	0.08249	1
	1.29	7	0.09123	0.09114	0.9990
	1.90	9	0.09414	0.09659	NO
SSE	1.14	5	0.08208	0.08219	1
	1.91	7	0.09140	0.09146	1
	1.68	9	0.09564	0.09875	NO
S	1.27	5	0.08230	0.08248	1
	2.21	7	0.09147	0.09157	1
	2.75	9	0.09752	0.09384	0.9623
N2 / 0.6345					
NNE	1.36	5	0.2014	0.1966	0.9762
	2.76	7	0.2725	0.2720	0.9982
	3.49	9	0.2854	0.2858	1
NE	1.17	5	0.2093	0.2031	0.9704
	2.32	7	0.2722	0.2723	1
	3.53	9	0.2862	0.2877	NO
ENE	1.02	5	0.1940	0.1878	0.9680
	1.92	7	0.2708	0.2710	1
	2.97	9	0.2870	0.2869	0.9997
E	0.92	5	0.2267	0.2187	0.9647
	1.37	7	0.2696	0.2695	0.9996
	2.24	9	0.2853	0.2852	0.9996
ESE	0.88	5	0.2412	0.2350	0.9743
	1.40	7	0.2673	0.2686	1
	2.13	9	0.2840	0.2841	1
SE	1.00	5	0.2515	0.2502	0.9948
	1.29	7	0.2670	0.2672	1
	1.90	9	0.2831	0.2831	1
SSE	1.14	5	0.2541	0.2533	0.9969
	1.91	7	0.2678	0.2679	1

(*continued on next page*)

Table B.1 (*continued*)

Point / Depth (m)	H_{morf} (m)	T (s)	H_B (m)	H_V (m)	K_d
	1.68	9	0.2826	0.2831	1
S	1.27	5	0.2534	0.2523	0.9957
	2.21	7	0.2685	0.2685	1
	2.75	9	0.2836	0.2837	1
N3 / 1.338					
NNE	1.36	5	0.2234	0.2164	0.9687
	2.76	7	0.5010	0.4920	0.9820
	3.49	9	0.5281	0.5286	1
NE	1.17	5	0.2343	0.2265	0.9667
	2.32	7	0.4897	0.4675	0.9547
	3.53	9	0.5283	0.5277	0.9989
ENE	1.02	5	0.2328	0.2243	0.9635
	1.92	7	0.4852	0.4674	0.9633
	2.97	9	0.5301	0.5294	0.9987
E	0.92	5	0.2662	0.2564	0.9632
	1.37	7	0.4508	0.4264	0.9459
	2.24	9	0.5293	0.5261	0.9940
ESE	0.88	5	0.2949	0.2821	0.9566
	1.40	7	0.4954	0.4812	0.9713
	2.13	9	0.5315	0.5300	0.9972
SE	1.00	5	0.3532	0.3380	0.9570
	1.29	7	0.4964	0.4801	0.9672
	1.90	9	0.5319	0.5307	0.9977
SSE	1.14	5	0.3855	0.3683	0.9554
	1.91	7	0.5202	0.5188	0.9973
	1.68	9	0.5315	0.5310	0.9991
S	1.27	5	0.3733	0.3567	0.9555
	2.21	7	0.5210	0.5201	0.9983
	2.75	9	0.5342	0.5346	1
N4 / 2.007					
NNE	1.36	5	0.2486	0.2397	0.9642
	2.76	7	0.6320	0.5877	0.9299
	3.49	9	0.7184	0.7052	0.9816
NE	1.17	5	0.2662	0.2562	0.9624
	2.32	7	0.5645	0.5149	0.9121
	3.53	9	0.7187	0.7055	0.9816
ENE	1.02	5	0.2632	0.2532	0.9620
	1.92	7	0.5368	0.4947	0.9216
	2.97	9	0.7228	0.7097	0.9819
E	0.92	5	0.2903	0.2788	0.9604
	1.37	7	0.4801	0.4479	0.9329
	2.24	9	0.7031	0.6711	0.9545
ESE	0.88	5	0.3151	0.3021	0.9587
	1.40	7	0.5578	0.5148	0.9229
	2.13	9	0.7305	0.7002	0.9585
SE	1.00	5	0.3758	0.3581	0.9529
	1.29	7	0.5591	0.5164	0.9236
	1.90	9	0.7352	0.7089	0.9642
SSE	1.14	5	0.4136	0.3923	0.9485
	1.91	7	0.7162	0.6888	0.9617
	1.68	9	0.7262	0.6922	0.9532
S	1.27	5	0.4023	0.3820	0.9495
	2.21	7	0.7256	0.7030	0.9689
	2.75	9	0.7574	0.7470	0.9863
N5 / 2.575					
NNE	1.36	5	0.2843	0.2766	0.9729
	2.76	7	0.7260	0.6797	0.9362
	3.49	9	0.9007	0.8768	0.9735
NE	1.17	5	0.3042	0.2955	0.9714
	2.32	7	0.6207	0.5778	0.9309
	3.53	9	0.9015	0.8809	0.9771
ENE	1.02	5	0.3059	0.2973	0.9719
	1.92	7	0.5783	0.5510	0.9528
	2.97	9	0.9101	0.8855	0.9730
E	0.92	5	0.3267	0.3173	0.9712
	1.37	7	0.5028	0.4674	0.9296
	2.24	9	0.8261	0.7548	0.9137
ESE	0.88	5	0.3489	0.3383	0.9696
	1.40	7	0.5562	0.5216	0.9378
	2.13	9	0.8306	0.7814	0.9408
SE	1.00	5	0.4044	0.3900	0.9644

(*continued on next page*)

Table B.1 (*continued*)

Point / Depth (m)	H_{morf} (m)	T (s)	H_B (m)	H_V (m)	K_d
	1.29	7	0.5656	0.5305	0.9379
	1.90	9	0.8329	0.7697	0.9241
SSE	1.14	5	0.4396	0.4221	0.9602
	1.91	7	0.8252	0.7706	0.9338
	1.68	9	0.7931	0.7319	0.9228
S	1.27	5	0.4314	0.4145	0.9608
	2.21	7	0.8596	0.8091	0.9413
	2.75	9	0.9610	0.9335	0.9714
N6 / 3.141					
NNE	1.36	5	0.3213	0.3155	0.9819
	2.76	7	0.8081	0.7672	0.9494
	3.49	9	1.093	1.052	0.9625
NE	1.17	5	0.3435	0.3369	0.9808
	2.32	7	0.7338	0.6961	0.9486
	3.53	9	1.106	1.072	0.9693
ENE	1.02	5	0.3363	0.3301	0.9816
	1.92	7	0.6442	0.6147	0.9542
	2.97	9	1.088	1.045	0.9605
E	0.92	5	0.3413	0.3348	0.9810
	1.37	7	0.5142	0.4951	0.9629
	2.24	9	0.8755	0.8277	0.9454
ESE	0.88	5	0.3510	0.3438	0.9795
	1.40	7	0.5521	0.5283	0.9569
	2.13	9	0.8377	0.7982	0.9528
SE	1.00	5	0.3969	0.3871	0.9753
	1.29	7	0.5274	0.5041	0.9558
	1.90	9	0.7855	0.7384	0.9400
SSE	1.14	5	0.4273	0.4152	0.9717
	1.91	7	0.7878	0.7391	0.9382
	1.68	9	0.7357	0.6916	0.9401
S	1.27	5	0.4226	0.4105	0.9714
	2.21	7	0.8474	0.7932	0.9360
	2.75	9	1.046	0.9927	0.9490
N7 / 3.844					
NNE	1.36	1.36	1.36	1.36	1.36
	2.76	2.76	2.76	2.76	2.76
	3.49	3.49	3.49	3.49	3.49
NE	1.17	1.17	1.17	1.17	1.17
	2.32	2.32	2.32	2.32	2.32
	3.53	3.53	3.53	3.53	3.53
ENE	1.02	1.02	1.02	1.02	1.02
	1.92	1.92	1.92	1.92	1.92
	2.97	2.97	2.97	2.97	2.97
E	0.92	0.92	0.92	0.92	0.92
	1.37	1.37	1.37	1.37	1.37
	2.24	2.24	2.24	2.24	2.24
ESE	0.88	0.88	0.88	0.88	0.88
	1.40	1.40	1.40	1.40	1.40
	2.13	2.13	2.13	2.13	2.13
SE	1.00	1.00	1.00	1.00	1.00
	1.29	1.29	1.29	1.29	1.29
	1.90	1.90	1.90	1.90	1.90
SSE	1.14	1.14	1.14	1.14	1.14
	1.91	1.91	1.91	1.91	1.91
	1.68	1.68	1.68	1.68	1.68
S	1.27	1.27	1.27	1.27	1.27
	2.21	2.21	2.21	2.21	2.21
	2.75	2.75	2.75	2.75	2.75
N8 / 4.391					
NNE	1.36	5	0.3836	0.3812	0.9937
	2.76	7	0.9192	0.8996	0.9787
	3.49	9	1.348	1.314	0.9748
NE	1.17	5	0.4078	0.4052	0.9936
	2.32	7	0.8955	0.8769	0.9792
	3.53	9	1.438	1.400	0.9736
ENE	1.02	5	0.3930	0.3906	0.9939
	1.92	7	0.7376	0.7237	0.9812
	2.97	9	1.274	1.240	0.9733
E	0.92	5	0.3764	0.3742	0.9942
	1.37	7	0.5735	0.5654	0.9859
	2.24	9	0.9689	0.9454	0.9757

(*continued on next page*)

Table B.1 (*continued*)

Point / Depth (m)	H_{morf} (m)	T (s)	H_B (m)	H_V (m)	K_d
ESE	0.88	5	0.3614	0.3591	0.9936
	1.40	7	0.5642	0.5568	0.9869
	2.13	9	0.8542	0.8369	0.9797
SE	1.00	5	0.3835	0.3807	0.9927
	1.29	7	0.4955	0.4878	0.9845
	1.90	9	0.7157	0.6976	0.9747
SSE	1.14	5	0.3954	0.3920	0.9914
	1.91	7	0.6894	0.6726	0.9756
	1.68	9	0.6385	0.6227	0.9753
S	1.27	5	0.3857	0.3823	0.9912
	2.21	7	0.7329	0.7137	0.9738
	2.75	9	1.001	0.9679	0.9669
N9 / 5.125					
NNE	1.36	5	0.4102	0.4091	0.9973
	2.76	7	0.9568	0.9477	0.9905
	3.49	9	1.433	1.414	0.9867
NE	1.17	5	0.4344	0.4333	0.9975
	2.32	7	0.9487	0.9398	0.9906
	3.53	9	1.565	1.543	0.9859
ENE	1.02	5	0.4160	0.4150	0.9976
	1.92	7	0.8071	0.8005	0.9918
	2.97	9	1.326	1.308	0.9864
E	0.92	5	0.3934	0.3925	0.9977
	1.37	7	0.5939	0.5904	0.9941
	2.24	9	0.9827	0.9725	0.9896
ESE	0.88	5	0.3720	0.3712	0.9978
	1.40	7	0.5719	0.5685	0.9941
	2.13	9	0.8375	0.8335	0.9952
SE	1.00	5	0.3896	0.3886	0.9974
	1.29	7	0.4832	0.4806	0.9946
	1.90	9	0.6760	0.6701	0.9913
SSE	1.14	5	0.3994	0.3983	0.9972
	1.91	7	0.6582	0.6529	0.9919
	1.68	9	0.5946	0.5898	0.9919
S	1.27	5	0.3898	0.3887	0.9972
	2.21	7	0.6966	0.6904	0.9911
	2.75	9	0.9361	0.9238	0.9869
N10 / 5.840					
NNE	1.36	5	0.4347	0.4346	0.9998
	2.76	7	0.9795	0.9786	0.9991
	3.49	9	1.471	1.469	0.9986
NE	1.17	5	0.4576	0.4575	0.9998
	2.32	7	0.9756	0.9746	0.9990
	3.53	9	1.595	1.586	0.9944
ENE	1.02	5	0.4359	0.4358	0.9998
	1.92	7	0.8533	0.8526	0.9992
	2.97	9	1.390	1.388	0.9986
E	0.92	5	0.4109	0.4108	0.9998
	1.37	7	0.6083	0.6080	0.9995
	2.24	9	1.009	1.008	0.9990
ESE	0.88	5	0.3890	0.3889	0.9997
	1.40	7	0.5880	0.5876	0.9993
	2.13	9	0.8555	0.8575	1
SE	1.00	5	0.4094	0.4093	0.9998
	1.29	7	0.5001	0.4999	0.9996
	1.90	9	0.7034	0.7035	1
SSE	1.14	5	0.4236	0.4235	0.9998
	1.91	7	0.6860	0.6854	0.9991
	1.68	9	0.6151	0.6146	0.9992
S	1.27	5	0.4154	0.4153	0.9998
	2.21	7	0.7260	0.7253	0.9990
	2.75	9	0.9649	0.9635	0.9985

Table B.2
Results in the output points along the central transect; 'NO' means no attenuation for those specific wave conditions; the points are shown on Fig. 7.

Point / Depth (m)	H_{morf} (m)	T (s)	H_B (m)	H_V (m)	K_d
C1 / 0.1346					
NNE	1.36	5	0.06530	0.06520	0.9985
	2.76	7	0.06251	0.06326	NO
	3.49	9	0.05953	0.05841	0.9812
NE	1.17	5	0.06521	0.06533	1
	2.32	7	0.06630	0.06568	0.9906
	3.53	9	0.06581	0.07238	NO
ENE	1.02	5	0.06510	0.06523	1
	1.92	7	0.07334	0.07335	1
	2.97	9	0.08018	0.08018	1
E	0.92	5	0.06508	0.06522	1
	1.37	7	0.07310	0.07306	0.9995
	2.24	9	0.07982	0.07986	1
ESE	0.88	5	0.06516	0.06529	1
	1.40	7	0.07294	0.07295	1
	2.13	9	0.07944	0.07967	1
SE	1.00	5	0.06496	0.06510	1
	1.29	7	0.07289	0.07288	0.9999
	1.90	9	0.07425	0.07736	NO
SSE	1.14	5	0.06512	0.06526	1
	1.91	7	0.07301	0.07300	0.9999
	1.68	9	0.07554	0.07967	NO
S	1.27	5	0.06560	0.06578	1
	2.21	7	0.07314	0.07325	1
	2.75	9	0.07855	0.07296	0.9288
C2 / 0.7394					
NNE	1.36	5	0.3073	0.3047	0.9915
	2.76	7	0.3223	0.3245	NO
	3.49	9	0.3404	0.3403	0.9997
NE	1.17	5	0.3077	0.3054	0.9925
	2.32	7	0.3261	0.3264	1
	3.53	9	0.3411	0.3460	NO
ENE	1.02	5	0.3045	0.3017	0.9908
	1.92	7	0.3277	0.3278	1
	2.97	9	0.3466	0.3466	1
E	0.92	5	0.3002	0.2967	0.9883
	1.37	7	0.3259	0.3259	1
	2.24	9	0.3460	0.3460	1
ESE	0.88	5	0.2931	0.2888	0.9853
	1.40	7	0.3242	0.3242	1
	2.13	9	0.3441	0.3440	0.9997
SE	1.00	5	0.2952	0.2913	0.9868
	1.29	7	0.3238	0.3238	1
	1.90	9	0.3425	0.3426	1
SSE	1.14	5	0.2947	0.2906	0.9861
	1.91	7	0.3236	0.3237	1
	1.68	9	0.3419	0.3424	1
S	1.27	5	0.2842	0.2787	0.9806
	2.21	7	0.3243	0.3243	1
	2.75	9	0.3429	0.3419	0.9971
C3 / 1.562					
NNE	1.36	5	0.4161	0.3969	0.9539
	2.76	7	0.6436	0.6422	0.9978
	3.49	9	0.6610	0.6594	0.9976
NE	1.17	5	0.4287	0.4085	0.9529
	2.32	7	0.6442	0.6425	0.9974
	3.53	9	0.6618	0.6619	1
ENE	1.02	5	0.4061	0.3871	0.9532
	1.92	7	0.6443	0.6405	0.9941
	2.97	9	0.6632	0.6614	0.9973
E	0.92	5	0.3859	0.3690	0.9562
	1.37	7	0.6103	0.5905	0.9676
	2.24	9	0.6609	0.6591	0.9973
ESE	0.88	5	0.3608	0.3463	0.9598
	1.40	7	0.6034	0.5838	0.9675
	2.13	9	0.6557	0.6526	0.9953
SE	1.00	5	0.3715	0.3559	0.9580
	1.29	7	0.5568	0.5281	0.9485
	1.90	9	0.6478	0.6433	0.9931
SSE	1.14	5	0.3720	0.3561	0.9573
	1.91	7	0.6198	0.6100	0.9842

(*continued on next page*)

Table B.2 (*continued*)

Point / Depth (m)	H_{morf} (m)	T (s)	H_B (m)	H_V (m)	K_d
	1.68	9	0.6424	0.6337	0.9865
S	1.27	5	0.3407	0.3270	0.9598
	2.21	7	0.6203	0.6110	0.9850
	2.75	9	0.6473	0.6457	0.9975
C4 / 2.354					
NNE	1.36	5	0.4474	0.4293	0.9595
	2.76	7	0.9481	0.9221	0.9726
	3.49	9	0.9877	0.9722	0.9843
NE	1.17	5	0.4595	0.4407	0.9591
	2.32	7	0.9372	0.9077	0.9685
	3.53	9	0.9891	0.9744	0.9851
ENE	1.02	5	0.4233	0.4075	0.9627
	1.92	7	0.9012	0.8556	0.9494
	2.97	9	0.9901	0.9743	0.9840
E	0.92	5	0.4040	0.3897	0.9646
	1.37	7	0.6991	0.6513	0.9316
	2.24	9	0.9750	0.9526	0.9770
ESE	0.88	5	0.3809	0.3685	0.9674
	1.40	7	0.6816	0.6378	0.9357
	2.13	9	0.9508	0.9186	0.9661
SE	1.00	5	0.3884	0.3756	0.9670
	1.29	7	0.5804	0.5466	0.9418
	1.90	9	0.8901	0.8408	0.9446
SSE	1.14	5	0.3896	0.3767	0.9669
	1.91	7	0.7828	0.7320	0.9351
	1.68	9	0.8127	0.7545	0.9284
S	1.27	5	0.3604	0.3492	0.9689
	2.21	7	0.7892	0.7379	0.9350
	2.75	9	0.9446	0.9224	0.9765
C5 / 3.119					
NNE	1.36	5	0.4730	0.4591	0.9706
	2.76	7	1.144	1.096	0.9580
	3.49	9	1.244	1.218	0.9791
NE	1.17	5	0.4834	0.4690	0.9702
	2.32	7	1.109	1.054	0.9504
	3.53	9	1.248	1.224	0.9808
ENE	1.02	5	0.4529	0.4394	0.9702
	1.92	7	1.002	0.9378	0.9359
	2.97	9	1.254	1.221	0.9737
E	0.92	5	0.4266	0.4164	0.9761
	1.37	7	0.7016	0.6668	0.9504
	2.24	9	1.178	1.118	0.9491
ESE	0.88	5	0.3984	0.3900	0.9789
	1.40	7	0.6785	0.6468	0.9533
	2.13	9	1.073	1.007	0.9385
SE	1.00	5	0.4067	0.3984	0.9796
	1.29	7	0.5757	0.5533	0.9611
	1.90	9	0.9187	0.8669	0.9436
SSE	1.14	5	0.4112	0.4028	0.9796
	1.91	7	0.8023	0.7620	0.9498
	1.68	9	0.8114	0.7696	0.9485
S	1.27	5	0.3837	0.3762	0.9805
	2.21	7	0.8160	0.7743	0.9489
	2.75	9	1.132	1.077	0.9514
C6 / 3.974					
NNE	1.36	5	0.4916	0.4805	0.9774
	2.76	7	1.226	1.176	0.9592
	3.49	9	1.361	1.330	0.9772
NE	1.17	5	0.4977	0.4865	0.9775
	2.32	7	1.172	1.116	0.9522
	3.53	9	1.364	1.335	0.9787
ENE	1.02	5	0.4687	0.4594	0.9802
	1.92	7	1.033	0.9791	0.9478
	2.97	9	1.347	1.310	0.9725
E	0.92	5	0.4390	0.4316	0.9831
	1.37	7	0.7163	0.6882	0.9608
	2.24	9	1.212	1.154	0.9521
ESE	0.88	5	0.4098	0.4041	0.9861
	1.40	7	0.6783	0.6558	0.9668
	2.13	9	1.068	1.019	0.9541
SE	1.00	5	0.4264	0.4209	0.9871

(*continued on next page*)

Table B.2 (*continued*)

Point / Depth (m)	H_{morf} (m)	T (s)	H_B (m)	H_V (m)	K_d
	1.29	7	0.5747	0.5596	0.9737
	1.90	9	0.9061	0.8695	0.9596
SSE	1.14	5	0.4413	0.4357	0.9873
	1.91	7	0.8078	0.7799	0.9655
	1.68	9	0.8059	0.7768	0.9639
S	1.27	5	0.4182	0.4131	0.9878
	2.21	7	0.8319	0.8021	0.9642
	2.75	9	1.195	1.145	0.9582
C7 / 4.364					
NNE	1.36	5	0.5024	0.4935	0.9823
	2.76	7	1.278	1.230	0.9624
	3.49	9	1.454	1.415	0.9732
NE	1.17	5	0.5045	0.4957	0.9826
	2.32	7	1.205	1.155	0.9585
	3.53	9	1.458	1.419	0.9733
ENE	1.02	5	0.4718	0.4646	0.9847
	1.92	7	1.052	1.006	0.9563
	2.97	9	1.432	1.394	0.9735
E	0.92	5	0.4421	0.4366	0.9876
	1.37	7	0.7155	0.6942	0.9702
	2.24	9	1.224	1.173	0.9583
ESE	0.88	5	0.4156	0.4115	0.9901
	1.40	7	0.6796	0.6627	0.9751
	2.13	9	1.067	1.027	0.9625
SE	1.00	5	0.4382	0.4344	0.9913
	1.29	7	0.5828	0.5720	0.9815
	1.90	9	0.9113	0.8843	0.9704
SSE	1.14	5	0.4607	0.4568	0.9915
	1.91	7	0.8254	0.8051	0.9754
	1.68	9	0.8188	0.7974	0.9739
S	1.27	5	0.4405	0.4368	0.9916
	2.21	7	0.8566	0.8346	0.9743
	2.75	9	1.239	1.198	0.9669
C8 / 4.483					
NNE	1.36	5	0.5062	0.4998	0.9874
	2.76	7	1.285	1.243	0.9673
	3.49	9	1.516	1.481	0.9769
NE	1.17	5	0.5028	0.4965	0.9875
	2.32	7	1.192	1.151	0.9656
	3.53	9	1.518	1.483	0.9769
ENE	1.02	5	0.466	0.461	0.9893
	1.92	7	1.017	0.9848	0.9683
	2.97	9	1.484	1.446	0.9744
E	0.92	5	0.4354	0.4316	0.9913
	1.37	7	0.6942	0.6797	0.9791
	2.24	9	1.201	1.162	0.9675
ESE	0.88	5	0.4114	0.4086	0.9932
	1.40	7	0.6732	0.6615	0.9826
	2.13	9	1.067	1.038	0.9728
SE	1.00	5	0.4395	0.4369	0.9941
	1.29	7	0.5956	0.5877	0.9867
	1.90	9	0.9481	0.9270	0.9777
SSE	1.14	5	0.4692	0.4663	0.9938
	1.91	7	0.8595	0.8435	0.9814
	1.68	9	0.8659	0.8485	0.9799
S	1.27	5	0.4519	0.4491	0.9938
	2.21	7	0.8976	0.8801	0.9805
	2.75	9	1.325	1.290	0.9736
C9 / 4.599					
NNE	1.36	5	0.5113	0.5075	0.9926
	2.76	7	1.261	1.232	0.9770
	3.49	9	1.603	1.576	0.9832
NE	1.17	5	0.5020	0.4984	0.9928
	2.32	7	1.161	1.134	0.9767
	3.53	9	1.618	1.593	0.9845
ENE	1.02	5	0.4595	0.4566	0.9937
	1.92	7	0.9734	0.9545	0.9806
	2.97	9	1.540	1.510	0.9805
E	0.92	5	0.4265	0.4243	0.9948
	1.37	7	0.6764	0.6680	0.9876
	2.24	9	1.178	1.152	0.9779

(*continued on next page*)

Table B.2 (*continued*)

Point / Depth (m)	H_{morf} (m)	T (s)	H_B (m)	H_V (m)	K_d
ESE	0.88	5	0.4042	0.4025	0.9958
	1.40	7	0.6724	0.6651	0.9891
	2.13	9	1.077	1.058	0.9824
SE	1.00	5	0.4373	0.4355	0.9959
	1.29	7	0.6113	0.6058	0.9910
	1.90	9	0.9887	0.9737	0.9848
SSE	1.14	5	0.4733	0.4713	0.9958
	1.91	7	0.8923	0.8808	0.9871
	1.68	9	0.9112	0.8984	0.9860
S	1.27	5	0.4602	0.4582	0.9957
	2.21	7	0.9355	0.9227	0.9863
	2.75	9	1.400	1.373	0.9807
C10 / 4.867					
NNE	1.36	5	0.5440	0.5424	0.9971
	2.76	7	1.269	1.256	0.9898
	3.49	9	1.810	1.790	0.9890
NE	1.17	5	0.5284	0.5269	0.9972
	2.32	7	1.166	1.155	0.9906
	3.53	9	1.883	1.863	0.9894
ENE	1.02	5	0.4738	0.4726	0.9975
	1.92	7	0.9586	0.9511	0.9922
	2.97	9	1.604	1.585	0.9882
E	0.92	5	0.4268	0.4260	0.9981
	1.37	7	0.6631	0.6598	0.9950
	2.24	9	1.128	1.118	0.9911
ESE	0.88	5	0.3939	0.3932	0.9982
	1.40	7	0.6504	0.6475	0.9955
	2.13	9	1.027	1.020	0.9932
SE	1.00	5	0.4209	0.4202	0.9983
	1.29	7	0.5904	0.5882	0.9963
	1.90	9	0.9493	0.9433	0.9937
SSE	1.14	5	0.4583	0.4575	0.9983
	1.91	7	0.8649	0.8602	0.9946
	1.68	9	0.8831	0.8779	0.9941
S	1.27	5	0.4498	0.4490	0.9982
	2.21	7	0.9123	0.9071	0.9943
	2.75	9	1.371	1.359	0.9912

Table B.3
Results in the output points along the south transect; 'NO' means no attenuation for those specific wave conditions; the points are shown on Fig. 7.

Point / Depth (m)	H_{morf} (m)	T (s)	H_B (m)	H_V (m)	K_d
S1 / 0.1313					
	1.36	5	0.03766	0.03784	1
NNE	2.76	7	0.03857	0.04205	NO
	3.49	9	0.04209	0.04158	0.9879
	1.17	5	0.0355	0.03548	0.9994
NE	2.32	7	0.03984	0.03982	0.9995
	3.53	9	0.05439	0.04353	0.8003
	1.02	5	0.03561	0.03562	1
ENE	1.92	7	0.04186	0.04168	0.9957
	2.97	9	0.04773	0.04776	1
	0.92	5	0.03587	0.03589	1
E	1.37	7	0.04203	0.04219	1
	2.24	9	0.0481	0.04814	1
	0.88	5	0.03629	0.03629	1
ESE	1.4	7	0.04254	0.04277	NO
	2.13	9	0.04773	0.04848	NO
	1	5	0.03683	0.03688	1
SE	1.29	7	0.04295	0.04296	1
	1.9	9	0.04798	0.04798	1
	1.14	5	0.03715	0.03713	0.9995
SSE	1.91	7	0.04375	0.04374	0.9998
	1.68	9	0.04794	0.04881	NO
	1.27	5	0.03732	0.03731	0.9997
S	2.21	7	0.0438	0.04391	1
	2.75	9	0.04771	0.04308	0.903
S2 / 0.5033					
NNE	1.36	5	0.2242	0.2242	1

(*continued on next page*)

Table B.3 (*continued*)

Point / Depth (m)	H_{morf} (m)	T (s)	H_B (m)	H_V (m)	K_d
	2.76	7	0.2349	0.2359	1
	3.49	9	0.2443	0.2438	0.998
	1.17	5	0.2239	0.2239	1
NE	2.32	7	0.2372	0.2373	1
	3.53	9	0.2478	0.2516	NO
	1.02	5	0.2218	0.2216	0.9991
ENE	1.92	7	0.2357	0.2358	1
	2.97	9	0.2512	0.2512	1
	0.92	5	0.2174	0.2172	0.9991
E	1.37	7	0.2316	0.2316	1
	2.24	9	0.2472	0.2472	1
	0.88	5	0.2107	0.2101	0.9972
ESE	1.4	7	0.2277	0.2275	0.9991
	2.13	9	0.243	0.2431	1
	1	5	0.2063	0.2058	0.9976
SE	1.29	7	0.2245	0.2244	0.9996
	1.9	9	0.2411	0.2407	0.9983
	1.14	5	0.2044	0.2041	0.9985
SSE	1.91	7	0.2246	0.2246	1
	1.68	9	0.2407	0.2402	0.9979
	1.27	5	0.1995	0.1989	0.997
S	2.21	7	0.2247	0.2245	0.9991
	2.75	9	0.2407	0.2391	0.9934
S3 / 1.214					
	1.36	5	0.4357	0.4256	0.9768
NNE	2.76	7	0.5627	0.5629	1
	3.49	9	0.5862	0.586	0.9997
	1.17	5	0.4254	0.4157	0.9772
NE	2.32	7	0.5615	0.562	1
	3.53	9	0.5843	0.5841	0.9997
	1.02	5	0.399	0.3906	0.9789
ENE	1.92	7	0.5527	0.5516	0.998
	2.97	9	0.5764	0.5765	1
	0.92	5	0.3686	0.3614	0.9805
E	1.37	7	0.5221	0.5158	0.9879
	2.24	9	0.5644	0.5642	0.9996
	0.88	5	0.336	0.3301	0.9824
ESE	1.4	7	0.5185	0.5142	0.9917
	2.13	9	0.5551	0.5552	1
	1	5	0.3458	0.3404	0.9844
SE	1.29	7	0.5001	0.4936	0.987
	1.9	9	0.5526	0.5529	1
	1.14	5	0.3511	0.3456	0.9843
SSE	1.91	7	0.5257	0.5247	0.9981
	1.68	9	0.5517	0.5501	0.9971
	1.27	5	0.3117	0.3074	0.9862
S	2.21	7	0.5244	0.5228	0.9969
	2.75	9	0.5511	0.5513	1
S4 / 2.063					
	1.36	5	0.4266	0.4162	0.9756
NNE	2.76	7	0.904	0.8696	0.9619
	3.49	9	1.052	1.033	0.9819
	1.17	5	0.4153	0.4057	0.9769
NE	2.32	7	0.8472	0.8126	0.9592
	3.53	9	1.056	1.039	0.9839
	1.02	5	0.3921	0.3838	0.9788
ENE	1.92	7	0.7629	0.7292	0.9558
	2.97	9	1.028	1.005	0.9776
	0.92	5	0.3689	0.3618	0.9808
E	1.37	7	0.5846	0.5638	0.9644
	2.24	9	0.9501	0.9175	0.9657
	0.88	5	0.3451	0.3392	0.9829
ESE	1.4	7	0.6121	0.5901	0.9641
	2.13	9	0.9638	0.9326	0.9676
	1	5	0.3627	0.3565	0.9829
SE	1.29	7	0.5571	0.5389	0.9673
	1.9	9	0.9255	0.8918	0.9636
	1.14	5	0.3718	0.3653	0.9825
SSE	1.91	7	0.7598	0.7295	0.9601
	1.68	9	0.8224	0.7883	0.9585
	1.27	5	0.3328	0.3275	0.9841
S	2.21	7	0.7223	0.694	0.9608
	2.75	9	1.003	0.9755	0.9726

(*continued on next page*)

Table B.3 (*continued*)

Point / Depth (m)	H_{morf} (m)	T (s)	H_B (m)	H_V (m)	K_d
S5 / 3.754					
	1.36	5	0.4315	0.4269	0.9893
NNE	2.76	7	0.8946	0.8682	0.9705
	3.49	9	1.253	1.209	0.9649
	1.17	5	0.4205	0.4163	0.99
NE	2.32	7	0.8149	0.793	0.9731
	3.53	9	1.299	1.255	0.9661
	1.02	5	0.3983	0.3946	0.9907
ENE	1.92	7	0.7233	0.7058	0.9758
	2.97	9	1.152	1.112	0.9653
	0.92	5	0.377	0.3737	0.9912
E	1.37	7	0.558	0.5473	0.9808
	2.24	9	0.957	0.9264	0.968
	0.88	5	0.3548	0.352	0.9921
ESE	1.4	7	0.5884	0.5766	0.9799
	2.13	9	0.9929	0.9598	0.9667
	1	5	0.3749	0.3718	0.9917
SE	1.29	7	0.5388	0.5289	0.9816
	1.9	9	0.9282	0.8987	0.9682
	1.14	5	0.3856	0.3823	0.9914
SSE	1.91	7	0.7423	0.7234	0.9745
	1.68	9	0.7991	0.7767	0.972
	1.27	5	0.3466	0.3439	0.9922
S	2.21	7	0.7079	0.6905	0.9754
	2.75	9	1.106	1.066	0.9638
S6 / 4.940					
	1.36	5	0.4569	0.4548	0.9954
NNE	2.76	7	0.9281	0.9135	0.9843
	3.49	9	1.304	1.277	0.9793
	1.17	5	0.4454	0.4434	0.9955
NE	2.32	7	0.8465	0.8346	0.9859
	3.53	9	1.356	1.327	0.9786
	1.02	5	0.4223	0.4205	0.9957
ENE	1.92	7	0.7531	0.7432	0.9869
	2.97	9	1.182	1.158	0.9797
	0.92	5	0.4003	0.3985	0.9955
E	1.37	7	0.584	0.5775	0.9889
	2.24	9	0.9839	0.9645	0.9803
	0.88	5	0.3773	0.3756	0.9955
ESE	1.4	7	0.6188	0.611	0.9874
	2.13	9	1.032	1.009	0.9777
	1	5	0.3991	0.3971	0.995
SE	1.29	7	0.5698	0.5628	0.9877
	1.9	9	0.971	0.9504	0.9788
	1.14	5	0.4112	0.4089	0.9944
SSE	1.91	7	0.7843	0.7708	0.9828
	1.68	9	0.8375	0.8216	0.981
	1.27	5	0.3695	0.3676	0.9949
S	2.21	7	0.7505	0.7379	0.9832
	2.75	9	1.173	1.144	0.9753
S7 / 5.618					
	1.36	5	0.4884	0.4878	0.9988
NNE	2.76	7	0.9909	0.9859	0.995
	3.49	9	1.392	1.382	0.9928
	1.17	5	0.4757	0.4751	0.9987
NE	2.32	7	0.9061	0.902	0.9955
	3.53	9	1.45	1.439	0.9924
	1.02	5	0.4508	0.4503	0.9989
ENE	1.92	7	0.8055	0.8019	0.9955
	2.97	9	1.251	1.241	0.992
	0.92	5	0.4307	0.43	0.9984
E	1.37	7	0.6296	0.6269	0.9957
	2.24	9	1.043	1.034	0.9914
	0.88	5	0.4111	0.4104	0.9983
ESE	1.4	7	0.6751	0.6715	0.9947
	2.13	9	1.104	1.094	0.9909
	1	5	0.4412	0.4402	0.9977
SE	1.29	7	0.6291	0.6256	0.9944
	1.9	9	1.053	1.043	0.9905
	1.14	5	0.4603	0.4592	0.9976
SSE	1.91	7	0.8757	0.8687	0.992
	1.68	9	0.9186	0.9107	0.9914

(*continued on next page*)

Table B.3 (*continued*)

Point / Depth (m)	H_{morf} (m)	T (s)	H_B (m)	H_V (m)	K_d
	1.27	5	0.4193	0.4184	0.9979
S	2.21	7	0.8497	0.8429	0.992
	2.75	9	1.311	1.296	0.9886
S8 / 6.095					
	1.36	5	0.5176	0.5176	1
NNE	2.76	7	1.057	1.057	1
	3.49	9	1.475	1.475	1
	1.17	5	0.5027	0.5027	1
NE	2.32	7	0.9636	0.9636	1
	3.53	9	1.534	1.534	1
	1.02	5	0.4742	0.4742	1
ENE	1.92	7	0.8484	0.8484	1
	2.97	9	1.304	1.304	1
	0.92	5	0.4551	0.4551	1
E	1.37	7	0.6618	0.6618	1
	2.24	9	1.079	1.079	1
	0.88	5	0.4391	0.4391	1
ESE	1.4	7	0.715	0.715	1
	2.13	9	1.146	1.146	1
	1	5	0.4779	0.4779	1
SE	1.29	7	0.6724	0.6724	1
	1.9	9	1.103	1.103	1
	1.14	5	0.5044	0.5044	1
SSE	1.91	7	0.945	0.945	1
	1.68	9	0.9733	0.9732	0.9999
	1.27	5	0.4658	0.4658	1
S	2.21	7	0.9289	0.9289	1
	2.75	9	1.412	1.412	1
	1.36	5	0.5477	0.5477	1
NNE	2.76	7	1.134	1.134	1
	3.49	9	1.577	1.577	1
	1.17	5	0.5292	0.5292	1
NE	2.32	7	1.029	1.029	1
	3.53	9	1.63	1.63	1
	1.02	5	0.4937	0.4937	1
ENE	1.92	7	0.8864	0.8864	1
	2.97	9	1.349	1.349	1
	0.92	5	0.4701	0.4701	1
E	1.37	7	0.6763	0.6763	1
	2.24	9	1.078	1.078	1
	0.88	5	0.4525	0.4525	1
ESE	1.4	7	0.7247	0.7247	1
	2.13	9	1.131	1.131	1
	1	5	0.4942	0.4942	1
SE	1.29	7	0.6849	0.6849	1
	1.9	9	1.097	1.097	1
	1.14	5	0.5251	0.5251	1
SSE	1.91	7	0.9724	0.9724	1
	1.68	9	0.9822	0.9822	1
	1.27	5	0.4894	0.4894	1
S	2.21	7	0.9699	0.9699	1
	2.75	9	1.455	1.455	1
S10 / 7.068					
	1.36	5	0.5997	0.5997	1
NNE	2.76	7	1.224	1.224	1
	3.49	9	1.686	1.686	1
	1.17	5	0.5716	0.5716	1
NE	2.32	7	1.102	1.102	1
	3.53	9	1.733	1.733	1
	1.02	5	0.5203	0.5203	1
ENE	1.92	7	0.9261	0.9261	1
	2.97	9	1.399	1.399	1
	0.92	5	0.4855	0.4855	1
E	1.37	7	0.69	0.69	1
	2.24	9	1.08	1.08	1
	0.88	5	0.4638	0.4638	1
ESE	1.4	7	0.7375	0.7375	1
	2.13	9	1.121	1.121	1
	1	5	0.5106	0.5106	1
SE	1.29	7	0.7061	0.7061	1
	1.9	9	1.104	1.104	1
	1.14	5	0.5496	0.5496	1
SSE	1.91	7	1.021	1.021	1

(*continued on next page*)

Table B.3 (*continued*)

Point / Depth (m)	H_{morf} (m)	T (s)	H_B (m)	H_V (m)	K_d
	1.68	9	1.009	1.009	1
	1.27	5	0.5204	0.5204	1
S	2.21	7	1.041	1.041	1
	2.75	9	1.533	1.533	1

Appendix C. Calculation of Wave Agitation and Wave Energy for the Baseline and Vegetation scenarios, in order to assess the impact of the Zostera noltei meadow

In this section we give an example of calculating the Wave Agitation and Wave Energy in one of the output points shown in Fig. 7, for which the results of the SWAN simulations were extracted. This example is mentioned in the section 4.2.

Let's consider the point C8, on the central transect, and the waves from NE.

Wave Agitation and Wave Energy for the Baseline Scenario and the Vegetation Scenario can be calculated using the formulae from Section 3.5. H_{Bi} and H_{Vi} are taken from Table B.2 in Appendix B, for the central transect, and f_i are taken from Table A.2 in Appendix A, for the NE waves.

For the Baseline Scenario, the wave heights that must be taken into account are: 0.5028 m, corresponding to the wave period of 5 s; 1.192 m, corresponding to the wave period of 7 s; 1.518 m, corresponding to the wave period of 9 s.

The frequencies of occurrence for the Baseline Scenario that must be taken into account are: 0.03162 for the wave heights between 0.5 and 1 m, corresponding to the wave period of 5 s; 0.00406 for the wave heights between 1 and 1.5 m, corresponding to the wave period of 7 s; 0.00007 for the wave heights between 1.5 and 2 m, corresponding to the wave period of 9 s.

Thus, the Wave Agitation from NE for the Baseline Scenario is:

$$WA_{B,NE} = 0.5028^{*}0.03162 + 1.192^{*}0.00406 + 1.518^{*}0.00007 = 0.020844 \text{ m}$$

The Wave Energy density per unit horizontal area from NE for the Baseline Scenario is:

$$WE_{B,NE} = (1/16)^{*}9.81^{*}1015^{*}\left(0.5028^{2^{*}}\ 0.03162 + 1.192^{2^{*}}\ 0.00406 + 1.518^{2^{*}}\ 0.00007\right) = 8.6651\ \text{J}/\text{m}^2$$

Similarly, for the Vegetation Scenario, the wave heights that must be taken into account are: 0.4965 m, corresponding to the wave period of 5 s; 1.151 m, corresponding to the wave period of 7 s; 1.483 m, corresponding to the wave period of 9 s.

The frequencies of occurrence for the Vegetation Scenario that must be taken into account are: 0.01601 for the wave heights between 0 and 0.5 m, corresponding to the wave period of 5 s; 0.00406 for the wave heights between 0.5 and 1 m, corresponding to the wave period of 7 s; 0.0003 for the wave heights between 1 and 1.5 m, corresponding to the wave period of 9 s.

Thus, the Wave Agitation from NE for the Vegetation Scenario is:

$$WA_{V,NE} = 0.4965^{*}0.01601 + 1.151^{*}0.00406 + 1.483^{*}0.00030 = 0.013067 \text{ m}$$

The Wave Energy density per unit horizontal area from NE for the Vegetation Scenario is:

$$WE_{B,NE} = (1/16)^{*}9.81^{*}1015^{*}\left(0.4965^{2^{*}}\ 0.01601 + 1.151^{2^{*}}\ 0.00406 + 1.483^{2^{*}}\ 0.00030\right) = 6.2140\ \text{J}/\text{m}^2$$

The Wave Agitation and the Wave Energy density per unit horizontal area for the other directions are computed in a similar manner. Finally, they are summed up for all the directions, in order to get the total Wave Agitation and Wave Energy density per unit horizontal area during a year.

References

Asano, T., Deguchi, H., Kobayashi, N., 1993. Interaction between water and vegetation. In: Proc. 23rd Int. Conf. Coast. Eng. Venice. ASCE, New York, pp. 2711–2723. https://doi.org/10.1061/9780872629332.206.

Avşar, N.B., Kutoğlu, Ş.H., 2020. Recent sea level change in the Black Sea from satellite altimetry and tide gauge observations. ISPRS Int. J. Geo-Inf. 2020 (9), 185. https://doi.org/10.3390/ijgi9030185.

Battjes, J., Janssen, J., 1978. Energy loss and set-up due to breaking of random waves. In: ASCE (ed.): Proc. 16th Int. Conf. Coastal Engineering, pp. 569–587. https://doi.org/10.1061/9780872621909.034.

Berov, D., Klayn, S., Deyanova, D., Karamfilov, V., 2022. Current distribution of Zostera seagrass meadows along the Bulgarian Black Sea coast (SW Black Sea, Bulgaria) (2010−2020). Biodivers. Data J. 10, e78942 https://doi.org/10.3897/BDJ.10.e78942.

Blackmar, P.J., Cox, D.T., Wei-Chang, W., 2014. Laboratory observations and numerical simulations of wave height attenuation in heterogeneous vegetation. J. Waterw. Port, Coast. Ocean Eng. 140 (1), 56–65. https://doi.org/10.1061/(ASCE)WW.1943-5460.0000215.

Bondar, C., 1989. Trends in the evolution of the mean Black Sea level. Meteorol. Hydrol. 19 (2), 23–28. Bucharest.

Booij, N., Ris, R.C., Holthuijsen, L.H., 1999. A third-generation wave model for coastal regions: 1. Model description and validation. J. Geophys. Res. 104 (c4), 7649–7666. https://doi.org/10.1029/98JC02622.

Bradley, K., Houser, C., 2009. Relative velocity of seagrass blades: Implications for wave attenuation in low-energy environments. J. Geophys. Res. 114, F01004. https://doi.org/10.1029/2007JF000951.

Casas-Prat, M., Sierra, J.P., 2010. Trend analysis of wave storminess: wave direction and its impact on harbour agitation. Nat. Hazards Earth Syst. Sci. 10 (2327–2340), 2010. www.nat-hazards-earth-syst-sci.net/10/2327/2010/doi:10.5194/nhess-10-2327-2010.

Cazenave, A., Le Cozannet, G., 2013. Sea level rise and its coastal impacts. Earth's Future 2, 15–34. https://doi.org/10.1002/2013EF000188.

Chen, S.N., Sanford, L.P., Koch, E.W., Shi, F., North, E.W., 2007. A nearshore model to investigate the effects of seagrass bed geometry on wave attenuation and suspended sediment transport. Estuar. Coasts 30 (2), 296–310. https://doi.org/10.1007/BF02700172.

Chen, X., Zhang, X., Church, J.A., Watson, C.S., King, M.A., Monselesan, D., Legresy, B., Harig, C., 2017. The increasing rate of global mean sea-level rise during 1993–2014. Nat. Clim. Change. Lett. https://doi.org/10.1038/NCLIMATE3325.

Church, J.A., Clark, P.U., Cazenave, A., Gregory, J.M., Jevrejeva, S., Levermann, A., Merrifield, M.A., Milne, G.A., Nerem, R.S., Nunn, P.D., Payne, A.J., Pfeffer, W.T., Stammer, D., Unnikrishnan, A.S., 2013. Sea Level Change. In: Stocker, T.F., Qin, D., Plattner, G.K., Tignor, M., Allen, S.K., Boschung, J., Nauels, A., Xia, Y., Bex, V., Midgley, P.M. (Eds.), Climate Change 2013: The Physical Science Basis. Contribution of Working Group I to the Fifth Assessment Report of the Intergovernmental Panel on Climate Change. Cambridge University Press, Cambridge, United Kingdom and New York, NY, USA, pp. 1137–1216.

Ciraolo, G., Ferreri, G.B., La Loggia, G., 2006. Flow resistance of *Posidonia oceanica* in shallow water. J. Hydraul. Res. 44 (2), 189–202. https://doi.org/10.1080/00221686.2006.9521675.

Colin, J., Déqué, M., Radu, R., Somot, S., 2010. Sensitivity study of heavy precipitation in Limited Area Model climate simulations: Influence of the size of the domain and the use of the spectral nudging technique. Tellus A 62, 591–604. https://doi.org/10.1111/j.1600-0870.2010.00467.x.

Constantinescu, Ş., Giosan, L., 2017. Marginal deltaic coasts in transition: From natural to anthropogenic along the southern Romanian cliffed coast. Anthropocene 19, 35–44. https://doi.org/10.1016/j.ancene.2017.08.005.

Curiel, D., Bellato, A., Rismondo, A., Marzocchi, M., 1996. Sexual reproduction of *Zostera noltii Hornemann* in the lagoon of Venice (Italy, north Adriatic). Aquat. Bot. 52, 313–318. https://doi.org/10.1016/0304-3770(95)00507-2.

Dalrymple, R., Kirby, J., Hwang, P., 1984. Wave diffraction due to areas of energy dissipation. J. Waterw. Port Coast. Ocean Eng. 110 (1), 67–79. https://doi.org/10.1061/(ASCE)0733-950X(1984)110:1(67).

Dee, D.P., Uppala, S.M., Simmons, A.J., Berrisford, P., Poli, P., Kobayashi, S., Andrae, U., Balmaseda, M.A., Balsamo, G., Bauer, D.P., Bechtold, P., 2011. The ERA-Interim reanalysis: Configuration and performance of the data assimilation system. Q. J. R. Meteorol. Soc. 137 (656), 553–597. https://doi.org/10.1002/qj.828.

del Estado, Puertos, 1994. ROM 0.3-91. Maritime Works Recommendations. Waves. Annex 1. Wave climate on the Spanish coast. Puertos del Estado. Ministry of Development. Government of Spain, p. 76.

Donatelli, C., Ganju, N.K., Kalra, T.S., Fagherazzi, S., Leonardi, N., 2019. Changes in hydrodynamics and wave energy as a result of seagrass decline along the shoreline of a microtidal back-barrier estuary. Adv. Water Resour. 128, 183–192. https://doi.org/10.1016/j.advwatres.2019.04.017.

Farda, A., Déué, M., Somot, S., Horányi, A., Spiridonov, V., Tóth, H., 2010. Model ALADIN as regional climate model for Central and Eastern Europe. Stud. Geophys. Geod. 54, 313–332. https://doi.org/10.1007/s11200-010-0017-7.

Feagin, R.A., Irish, J.L., Möller, I., Williams, A.M., Colón-Rivera, R.J., Mousavi, M.E., 2011. Short communication: Engineering properties of wetland plants with application to wave attenuation. Coast. Eng. 58, 251–255. https://doi.org/10.1016/j.coastaleng.2010.10.003.

Fonseca, M.S., Cahalan, J.H., 1992. A preliminary evaluation of wave attenuation by four species of seagrass. Estuar. Coast. Shelf Sci. 35 (6), 565–576.

Fonseca, M.S., Koehl, M.A.R., 2006. Flow in seagrass canopies: The influence of patch width. Estuar. Coast. Shelf Sci. 67, 1–9. https://doi.org/10.1016/j.ecss.2005.09.018.

Fonseca, M.S., Fisher, J.S., Zieman, J.C., Thayer, G.W., 1982. Influence of the seagrass, *Zostera marina L.*, on current flow. Estuar. Coast. Shelf Sci. 15 (4), 351–358. https://doi.org/10.1016/0272-7714(82)90046-4.

Foster-Martinez, M.R., Lacy, J.R., Ferner, M.C., Variano, E.A., 2018. Wave attenuation across a tidal marsh in San Francisco Bay. Coast. Eng. 136, 26–40. https://doi.org/10.1016/j.coastaleng.2018.02.001.

Fraschetti, S., Guarnieri, G., Bevilacqua, S., Terlizzi, A., Boero, F., 2013. Protection enhances community and habitat stability: evidence from a Mediterranean marine protected area. PLoS One 8 (12), e81838. https://doi.org/10.1371/journal.pone.0081838.

Ganthy, F., Sottolichio, A., Verney, R., 2013a. Seasonal modification of tidal flat sediment dynamics by seagrass meadows of *Zostera noltii* (Bassin d'Arcachon, France). J. Mar. Syst. 109-110, S233–S240. https://doi.org/10.1016/j.jmarsys.2011.11.027.

Ganthy, F., Verney, R., Sottolichio, A., 2013b. A numerical investigation on the effect of small and flexible seagrass *Zostera Noltii* on water flow. In: Coastal Dynamics 2013, Paper no. 077.

Ganthy, F., Soissons, L., Sauriau, P.G., Verney, R., Sottolichio, A., 2015. Effects of short flexible seagrass *Zostera Noltei* on flow, erosion and deposition processes determined using flume experiments. Sedimentology 62 (4), 997–1023. https://doi.org/10.1111/sed.12170.

Granata, T.C., Serra, T., Colomer, J., Casamitjana, X., Duarte, C.M., Gacia, E., 2001. Flow and particle distributions in a nearshore seagrass meadow before and after a storm. Mar. Ecol. Prog. Ser. 218, 95–106. https://doi.org/10.3354/meps218095.

HALCROW UK, GeoEcoMar, NIMRD 'Antipa', University of Bucharest, ISMAR-CNR, 2012. Master Plan for the Protection against Erosion and Rehabilitation of the Romanian Coastal Zone.

He, F., Chen, J., Jiang, C., 2019. Surface wave attenuation by vegetation with the stem, root and canopy. Coast. Eng. 152 https://doi.org/10.1016/j.coastaleng.2019.103509.

Hemer, M.A., Katzfey, J., Trenham, C., 2013. Global dynamical projections of surface ocean wave climate for a future high greenhouse gas emission scenario. Ocean Model 70, 221–245. https://doi.org/10.1016/j.ocemod.2012.09.008.

Herrmann, M., Somot, S., Calmanti, S., Dubois, C., Sevault, F., 2011. Representation of spatial and temporal variability of daily wind speed and of intense wind events over the Mediterranean Sea using dynamical downscaling: Impact of the regional climate model configuration. Nat. Hazards Earth Syst. Sci. 11, 1983–2001. https://doi.org/10.5194/nhess-11-1983-2011.

Holmer, M., Georgiev, V.G., Karamfilov, V.K., 2016. Effects of point source of untreated sewage waters on seagrass (*Zostera marina* and *Z. noltii*) beds in the South-Western Black Sea. Aquat. Bot. 133, 1–9. https://doi.org/10.1016/j.aquabot.2016.05.001.

Holthuijsen, L., 2007. Waves in oceanic and coastal waters. Cambridge University Press, Cambridge. https://doi.org/10.1017/CBO9780511618536.

Infantes, E., Orfila, A., Simarro, G., Terrados, J., Luhar, M., Nepf, H., 2012. Effect of a seagrass *(Posidonia oceanica)* meadow on wave propagation. Mar. Ecol. Prog. Ser. 456, 63–72. https://doi.org/10.3354/meps09754.

Jadhav, R.S., Chen, Q., Smith, J.M., 2013. Spectral distribution of wave energy dissipation by salt marsh vegetation. Coast. Eng. 77, 99–107. https://doi.org/10.1016/j.coastaleng.2013.02.013.

Japan International Cooperation Agency (JICA), 2008. The study on protection and rehabilitation of the Southern Romanian Black Sea shore in Romania, Draft Final Report, Vol. 1. Basic Study and Coastal Protection Plan.

Jevrejeva, S., Grinsted, A., Moore, J.C., 2014. Upper limit for sea level projections by 2100. Environ. Res. Lett. 9, 104008 https://doi.org/10.1088/1748-9326/9/10/104008.

Jiang, Z., Huang, D., Fang, Y., Cui, L., Zhao, C., Liu, S., Wu, Y., Chen, Q., Ranvilage, C.I.P. M., He, J., Huang, X., 2020. Home for marine species: seagrass leaves as vital spawning grounds and food source. Front. Mar. Sci. 7, 194. https://doi.org/10.3389/fmars.2020.00194.

John, B.M., Shirlal, K.G., Rao, S., 2015. Effect of artificial vegetation on wave attenuation – an experimental investigation. Procedia Eng. 116, 600–606. https://doi.org/10.1016/j.proeng.2015.08.331.

Kobayashi, N., Raichle, A.W., Asano, T., 1993. Wave attenuation by vegetation. J. Waterw. Port Coast. Ocean Eng. 119 (1), 30–48. https://doi.org/10.1061/(ASCE)0733-950X(1993)119:1(30).

Koch, E.W., Barbier, E.B., Silliman, B.R., Reed, D.J., Perillo, G.M.E., Hacker, S.D., Granek, E.F., Primavera, J.H., Muthiga, N., Polasky, S., Halpern, B.S., Kennedy, C.J., Kappel, C.V., Wolanski, E., 2009. Non-linearity in ecosystem services: temporal and spatial variability in coastal protection. Front. Ecol. Environ. 7 (1), 29–37. https://doi.org/10.1890/080126.

Koftis, T., Prinos, P., Stratigaki, V., 2013. Wave damping over artificial *Posidonia oceanica* meadow: a large-scale experimental study. Coast. Eng. 73 (1), 71–83. https://doi.org/10.1016/j.coastaleng.2012.10.007.

Kombiadou, K., Ganthy, F., Verney, R., Plus, M., Sottolichio, A., 2014. Modelling the effects of *Zostera noltei* meadows on sediment dynamics: application to the Arcachon lagoon. Ocean Dyn. 64, 1499–1516. https://doi.org/10.1007/s10236-014-0754-1.

la Hausse de Lalouvière, C., Gràcia, V., Sierra, J.P., Lin-Ye, J., García-León, M., 2020. Impact of climate change on nearshore waves at a beach protected by a barrier reef. Water 2020 (12), 1681. https://doi.org/10.3390/w12061681.

Larkum, A.W.D., Orth, R.J., Duarte, C.M., 2006. Seagrasses: Biology, Ecology and Conservation. Springer, USA, 691 p., ISBN-10 1-4020-2942-X.

Lin-Ye, J., García-León, M., Gràcia, V., Ortego, M.I., Stănică, A., Sánchez-Arcilla, A., 2018. Multivariate hybrid modelling of future wave-storms at the northwestern Black Sea. Water 10, 221. https://doi.org/10.3390/w10020221.

Losada, I.J., Maza, M., Lara, J.L., 2016. A new formulation for vegetation-induced damping under combined waves and currents. Coast. Eng. 107, 1–13. https://doi.org/10.1016/j.coastaleng.2015.09.011.

Lowe, R.J., Falter, J.L., Koseff, J.R., Monismith, S.G., Atkinson, M.J., 2007. Spectral wave flow attenuation within submerged canopies: Implications for wave energy dissipation. J. Geophys. Res. 112, C05018. https://doi.org/10.1029/2006JC003605.

Luhar, M., Coutu, S., Infantes, E., Fox, S., Nepf, H., 2010. Wave-induced velocities inside a model seagrass bed. J. Geophys. Res. 115, C12005. https://doi.org/10.1029/2010JC006345.

Luhar, M., Infantes, E., Orfila, A., Terrados, J., Nepf, H.M., 2013. Field observations of wave-induced streaming through a submerged seagrass (Posidonia oceanica) meadow. J. Geophys. Res.: Oceans 118. https://doi.org/10.1002/jgrc.20162.

Luhar, M., Infantes, E., Nepf, H., 2017. Seagrass blade motion under waves and its impact on wave decay. J. Geophys. Res.: Oceans 122. https://doi.org/10.1002/2017JC012731.

Ma, G., Shi, F., Kirby, J.T., 2012. Shock-capturing non-hydrostatic model for fully dispersive surface wave processes. Ocean Model 43-44, 22–35. https://doi.org/10.1016/j.ocemod.2011.12.002.

Ma, G., Kirby, J.T., Su, S.-F., Figlus, J., Shi, F., 2013. Numerical study of turbulence and wave damping induced by vegetation canopies. Coast. Eng. 80, 68–78. https://doi.org/10.1016/j.coastaleng.2013.05.007.

Ma, G., Han, Y., Niroomandi, A., Lou, S., Liu, S., 2015. Numerical study of sediment transport on a tidal flat with a patch of vegetation. Ocean Dyn. 65, 203–222. https://doi.org/10.1007/s10236-014-0804-8.

Madsen, O., Poon, Y., Graber, H., 1988. Spectral wave attenuation by bottom friction: Theory. In: In: ASCE (ed.): Proceedings of 21th International Conference in Coastal Engineering, pp. 492–504. https://doi.org/10.9753/ICCE.V21.34.

Manca, E., Stratigaki, V., Prinos, P., 2010. Large scale experiments on spectral wave propagation over *Posidonia oceanica* seagrass. In: Christodoulou, Stamou (Eds.), Environmental Hydraulics. Taylor & Francis Group/Balkema, London. https://doi.org/10.1201/b10553-74. ISBN 978-0-415-58475-3, 463-468.

Manca, E., Cáceres, I., Alsina, J.M., Stratigaki, V., Townend, I., Amos, C.L., 2012. Wave energy and wave-induced flow reduction by full-scale model *Posidonia oceanica* seagrass. Cont. Shelf Res. 50-51 (1), 100–116. https://doi.org/10.1016/j.csr.2012.10.008.

Marin, O., Abaza, V., Sava, D., 2013. Phytobenthos - Key biological element in shallow marine waters. Cercetări Marine 43 (1), 197–218. https://doi.org/10.55268/CM.2013.43.197.

Maza, M., Lara, J.L., Losada, I.J., 2016. Solitary wave attenuation by vegetation patches. Adv. Water Resour. 98, 159–172. https://doi.org/10.1016/j.advwatres.2016.10.021.

McIvor, A.L., Möller, I., Spencer, T., Spalding, M., 2012. Reduction of wind and swell waves by mangroves. Natural Coastal Protection Series: Report 1. Cambridge Coastal Research Unit Working Paper 40 (ISSN 2050-7941).

Mendez, F.J., Losada, I.J., 2004. An empirical model to estimate the propagation of random breaking and nonbreaking waves over vegetation fields. Coast. Eng. 51 (2), 103–118. https://doi.org/10.1016/j.coasaleng.2003.11.003.

Mendez, F.J., Losada, I.J., Losada, M.A., 1999. Hydrodynamics induced by wind waves in a vegetation field. J. Geophys. Res. 104 (C8), 18383–18396. https://doi.org/10.1029/1999JC900119.

Milchakova, N., Phillips, R., 2003. Black Sea seagrasses. Mar. Pollut. Bull. 46 (6), 695–699. https://doi.org/10.1016/S0025-326X(02)00361-2.

Möller, I., 2006. Quantifying saltmarsh vegetation and its effect on wave height dissipation: Results from a UK east coast saltmarsh. Estuar. Coast. Shelf Sci. 69 (3–4), 337–351. https://doi.org/10.1016/j.ecss.2006.05.003.

Möller, I., Spencer, T., 2002. Wave dissipation over macro-tidal saltmarshes: Effects of marsh edge typology and vegetation change. J. Coast. Res. https://doi.org/10.2112/1551-5036-36.sp1.506. Special Issue 36 (ICS 2002 Proceedings), ISSN 0749-0208, 506-521.

Möller, I., Kudella, M., Rupprecht, F., Spencer, T., Paul, M., van Wesenbeeck, B.K., Wolters, G., Jensen, K., Bouma, T.J., Miranda-Lange, M., Schimmels, S., 2014. Wave attenuation over coastal salt marshes under storm surge conditions. Nat. Geosci. 7 (10), 727–731. https://doi.org/10.1038/NGEO2251.

Monclús i Bori, A., Dinu, I., García-León, M., Lin-Ye, J., Gràcia, V., Stănică, A., 2019. First considerations on environmental friendly solutions to protect the southern Romanian coast. Geo-Eco-Marina 24, 57–68. http://hdl.handle.net/2117/131101.

Myrhaug, D., Holmedal, L.E., 2011. Drag force on a vegetation field due to longcrested and short-crested nonlinear random waves. Coast. Eng. 58, 562–566. https://doi.org/10.1016/j.coastaleng.2011.01.014.

Myrhaug, D., Holmedal, L.E., Ong, M.C., 2009. Nonlinear random wave-induced drag force on a vegetation field. Coast. Eng. 56, 371–376. https://doi.org/10.1016/j.coastaleng.2008.10.009.

Nepf, H., White, B., Lightbody, A., Ghisalberti, M., 2007. Transport in aquatic canopies. In: Gayev, Y.A., Hunt, J.C. (Eds.), Flow and Transport Processes with Complex Obstructions. NATO Science Series, vol 236. Springer, Dordrecht. https://doi.org/10.1007/978-1-4020-5385-6_6.

Nerem, R.S., Beckley, B.D., Fasullo, J.T., Hamlington, B.D., Masters, D., Mitchum, G.T., 2018. Climate-change-driven accelerated sea-level rise detected in the altimeter era. Proc. Natl. Acad. Sci. U. S. A. 115 (9) https://doi.org/10.1073/pnas.1717312115.

Newell, R.I.E., Koch, E.W., 2004. Modelling seagrass density and distribution in response to changes in turbidity stemming from bivalve filtration and seagrass sediment stabilization. Estuaries 27 (5), 793–806. https://doi.org/10.1007/BF02912041.

Niță, V., Micu, D., Nenciu, M., 2014. First attempt of transplanting the key-species *Cystoseira barbata* and *Zostera noltei* at the Romanian coast. Cercetări Marine 44, 147–163. https://doi.org/10.55268/CM.2014.44.147.

Nordlund, L.M., Jackson, E.L., Nakaoka, M., Samper-Villarreal, J., Beca-Carretero, P., Creed, J.C., 2017. Seagrass ecosystem services – What's next? Mar. Pollut. Bull. 134, 145–151. https://doi.org/10.1016/j.marpolbul.2017.09.014.

Ondiviela, B., Losada, I.J., Lara, J.L., Maza, M., Galván, C., Bouma, T.J., van Belzen, J., 2014. The role of seagrasses in coastal protection in a changing climate. Coast. Eng. 87, 158–168. https://doi.org/10.1016/j.coastaleng.2013.11.005.

Ota, T., Kobayashi, N., Kirby, J.T., 2004. Wave and current interactions with vegetation. In: Proc. Int. Conf. Coastal Eng. Lisbon, 508–520. ASCE, New York. https://doi.org/10.1142/9789812701916_0040.

Panin, N., 2005. The Black Sea coastal zone – an overview. Geo-Eco-Marina - European Seas: Coastal zones and Rivers - Sea System 11, 21–40. https://doi.org/10.5281/zenodo.57388.

Paul, M., Amos, C.L., 2011. Spatial and seasonal variation in wave attenuation over *Zostera noltii*. J. Geophys. Res. 116, C08019. https://doi.org/10.1029/2010JC006797.

Phillips, R.C., Milchakova, N.A., Alexandrov, V.V., 2006. Growth dynamics of *Zostera* in Sevastopol Bay (Crimea, Black Sea). Aquat. Bot. 85, 244–248. https://doi.org/10.1016/j.aquabot.2006.03.004.

Pinsky, M.L., Guannel, G., Arkema, K.K., 2013. Quantifying wave attenuation to inform coastal habitat conservation. Ecosphere 4 (8), 95. https://doi.org/10.1890/ES13-00080.1.

Price, W.A., Tomlinson, K.W., Hunt, J.N., 1968. The effect of artificial seaweed in promoting the build-up of beaches. In: Proc. 11th Conf. Coast. Eng. London, 570-578. ASCE, New York. https://doi.org/10.9753/ICCE.V11.36.

Ros, À., Colomer, J., Serra, T., Pujol, D., Soler, M., Casamitjana, X., 2014. Experimental observations on sediment resuspension within submerged model canopies under oscillatory flow. Cont. Shelf Res. 91, 220–231. https://doi.org/10.1016/j.csr.2014.10.004.

Ruangpan, L., Vojinovic, Z., Di Sabatino, S., Leo, L.S., Capobianco, V., Oen, A.M.P., McClain, M.E., Lopez-Gunn, E., 2020. Nature-based solutions for hydro-meteorological risk reduction: a state-of-the-art review of the research area. Nat. Hazards Earth Syst. Sci. 20, 243–270. https://doi.org/10.5194/nhess-20-243-2020.

Ruckelshaus, M.H., Guannel, G., Arkema, K., Verutes, G., Griffin, R., Guerry, A., Silver, J., Faries, J., Brenner, J., Rosenthal, A., 2016. Evaluating the benefits of green infrastructure for coastal areas: location, location, location. Coast. Manag. 44 (5), 504–516. https://doi.org/10.1080/08920753.2016.1208882.

Ruti, P.M., Somot, S., Giorgi, F., Dubois, C., Flaounas, E., Obermann, A., Dell'Aquila, A., Pisacane, G., Harzallah, A., Lombardi, E., et al., 2016. Med-CORDEX initiative for Mediterranean climate studies. Bull. Am. Meteorol. Soc. 97, 1187–1208. https://doi.org/10.1175/BAMS-D-14-00176.1.

Sánchez-Arcilla, A., García-León, M., Gràcia, V., Devoy, R., Stănică, A., Gault, J., 2016. Managing coastal environments under climate change: Pathways to adaptation. Sci. Total Environ. 572, 1336–1352. https://doi.org/10.1016/j.scitotenv.2016.01.124.

Sánchez-González, J.F., Sánchez-Rojas, V., Memos, C.D., 2011. Wave attenuation due to *Posidonia Oceanica* meadows. J. Hydraul. Res. 49 (4), 503–514. https://doi.org/10.1080/00221686.2011.552464.

Saunders, M.I., Leon, J., Phinn, S.R., Callaghan, D.P., O'Brien, K.R., Roelfsema, C.R., Lovelock, C.E., Lyons, M.B., Mumby, P.J., 2013. Coastal retreat and improved water quality mitigate losses of seagrass from sea level rise. Glob. Chang. Biol. 19 (8), 2569–2583. https://doi.org/10.1111/gcb.12218.

Scalpone, C.R., Jarvis, J.C., Vasslides, J.M., Testa, J.M., Ganju, N.K., 2020. Simulated estuary-wide response of seagrass (*Zostera marina*) to future scenarios of temperature and sea level. Front. Mar. Sci. 7, 539946 https://doi.org/10.3389/fmars.2020.539946.

Shore Protection Manual, 1984. U.S. Army Coastal Engineering Research Center, Department of the Army, Corps of Engineers, U.S. Govt. Printing Office, Washington, DC, USA.

Short, F.T., Carruthers, T.J.R., Waycott, M., Kendrick, G.A., Fourqurean, J.W., Callabine, A., Kenworthy, W.J., Dennison, W.C., 2010. *Zostera noltei.* The IUCN Red List of Threatened Species 2010: e.T173361A6999224. https://doi.org/10.2305/IUCN.UK.2010-3.RLTS.T173361A6999224.en.

Sierra, J.P., García-León, M., Gràcia, V., Sánchez-Arcilla, A., 2017. Green measures for Mediterranean harbours under a changing climate. Proc. Inst. Civ. Eng.: Marit. Eng 170 (2), 55–66. https://doi.org/10.1680/jmaen.2016.23.

Sorokin, I., 1982. The Black Sea. Ed. Nauka Acad. Sc, USSR, Moscow, p. 216.

Stocker, T.F., Qin, D., Plattner, G.K., Tignor, M., Allen, S.K., Boschung, J., Nauels, A., Xia, Y., Bex, V., Midgley, P.M., 2013. IPCC, 2013: Summary for Policymakers. Climate Change 2013: The physical science basis. In: Contribution of Working Group I to the Fifth Assessment Report of the Intergovernmental Panel on Climate Change. Cambridge University Press, Cambridge, UK; New York, NY, USA, p. 1535.

Surugiu, V., 2008. On the Occurrence of *Zostera noltei* Hornemann at the Romanian Coast of the Black Sea. Analele ştiinţifice ale Universităţii 'Al. I. Cuza' Iaşi LIV, fasc. 2, s.II (a. Biologie vegetală).

Surugiu, V., Teacă, A., Șvedu, I., Quijón, P.A., 2021. A hotspot in the Romanian Black Sea: Eelgrass beds drive local biodiversity in surrounding bare sediments. Front. Mar. Sci. https://doi.org/10.3389/fmars.2021.745137.

Sutton-Grier, A.E., Gittman, R.K., Arkema, K.K., Bennett, R.O., Benoit, J., Blitch, S., Burks-Copes, K.A., Colden, A., Dausman, A., DeAngelis, B.M., Hughes, A.R., Scyphers, S.B., Grabowski, J.H., 2018. Investing in natural and nature-based infrastructure: Building better along our coasts. Sustainability 10, 1–11. https://doi.org/10.3390/su10020523.

Suzuki, T., Zijlema, M., Burger, B., Meijer, M.C., Narayan, S., 2012. Wave dissipation by vegetation with layer schematization in SWAN. Coast. Eng. 59 (1), 64–71. https://doi.org/10.1016/j.coastaleng.2011.07.006.

Tătui, F., Pîrvan, M., Popa, M., Aydogan, B., Ayat, B., Görmüş, T., Korzinin, D., Văidianu, N., Vespremeanu-Stroe, A., Zăinescu, F., Kuznetsov, S., Preoteasa, L., Shtremel, M., Saprykina, Y., 2019. The Black Sea coastline erosion: Index-based sensitivity assessment and management-related issues. Ocean Coast. Manag. 182 https://doi.org/10.1016/j.ocecoaman.2019.104949.

U.S. Army Corps of Engineers, 2002. Coastal Engineering Manual.

Van Rooijen, A.A., McCall, R.T., Thiel, Van, de Vries, J.S.M., Van Dongeren, A.R., Reniers, A.J.H.M., Roelvink, J.A., 2016. Modeling the effect of wave-vegetation interaction on wave setup. J. Geophys. Res.: Oceans 121, 6, 4341–4359. https://doi.org/10.1002/2015JC011392.

Vuik, V., Jonkman, S.N., Borsje, B.W., Suzuki, T., 2016. Nature-based flood protection: The efficiency of vegetated foreshores for reducing wave loads on coastal dikes. Coast. Eng. 116, 42–56. https://doi.org/10.1016/j.coastaleng.2016.06.001.

Waycott, M., Collier, C., McMahon, K., Ralph, P., McKenzie, L., Udy, J., Grech, A., 2007. Vulnerability of seagrasses in the Great Barrier Reef to climate change. Chapter 8. Part II: Species and species groups. In: Johnson, J.E., Marshall, P.A. (Eds.), Climate Change and the Great Barrier Reef. Great Barrier Reef Marine Park Authority and Australian Greenhouse Office, Australia, p. 818.

Yankovsky, A.E., Lemeshko, E.M., Ilyin, Y.P., 2004. The influence of shelfbreak forcing on the alongshelf penetration of the Danube buoyant water. Black Sea. Cont. Shelf Res. 24, 1083–1098. https://doi.org/10.1016/j.csr.2004.03.007.

Yi, S., Sun, W., Heki, K., Qian, A., 2015. An increase in the rate of global mean sea level rise since 2010. Geophys. Res. Lett. 42 https://doi.org/10.1002/2015GL063902.